

# Deep Learning Technology-Based Exoskeleton Robot Controller Development

SK Hasan

Department of Mechanical and Manufacturing Engineering

Miami University

Oxford, OH 45056

**Word count:** 8,617

**Corresponding Author:**

**SK Hasan**

[hasansk@miamioh.edu](mailto:hasansk@miamioh.edu)

Department of Mechanical and Manufacturing Engineering

Miami University

Oxford, OH

OH 45056

# Deep Learning Technology-Based Exoskeleton Robot Controller Development

## Abstract:

Model-based control is preferred for robotics applications due to its systematic approach to linearize and control the robot's nonlinear dynamics. The fundamental challenge involved in implementing a model-based controller for robotics applications is the time delay associated with the real-time computation of the robot dynamics. Due to the sequential structure of the robot's dynamic equation of motion, the multicore CPU cannot reduce the control algorithm execution time. A high-speed processor is required to maintain a higher sampling rate. Neural network-based modeling offers an excellent solution for developing a parallel structured equivalent model of the sequential model that is suitable for parallel processing. In this paper, a Deep neural network-based parallel structured 7 degrees of freedom human lower extremity exoskeleton robot controller is developed. Forty-nine densely connected neurons are arranged in four layers to estimate joint torque requirements for tracking trajectories. For training, the deep neural network, an analytical model-based data generation technique is presented. A trained deep neural network is used for real-time joint torque prediction and a PD controller is incorporated to mitigate the prediction errors. Simulation results show high trajectory tracking performances. The developed controller's stability analysis is proved. The robustness of the controller against the parameter variation is analyzed with the help of the analysis of variance (ANOVA). A comparative study between the developed controller and the Computed Torque Controller, Model Reference Computed Torque Controller, Sliding Mode Controller, Adaptive controller, and Linear Quadratic Regulator are presented while keeping the same robot dynamics. The comparative study shows that the developed controller produced torque similar to other conventional controllers while maintaining small trajectory tracking errors.

**Keywords:** Deep learning robot control, Exoskeleton robot control, AI in dynamic control

# Exoskeleton Robot Controller Development Based on Deep Learning Technology

## 1. Introduction

Currently, there has been significant research focused on the advancement of exoskeleton robots. These remarkable machines have gained research attention due to their immense potential in augmenting human capabilities, revolutionize rehabilitation methods, and significantly enhance the quality of life for individuals facing mobility disabilities [1-3]. Functioning as wearable devices, exoskeleton robots amplify and assist human movements, facilitating activities like walking, lifting, and maintaining balance. Due to their effectiveness in augmenting human capabilities and introducing a new way for rehabilitation, an increasing number of researchers are directing their attention toward exoskeleton robots[4-6].

Robotics is an interdisciplinary branch of engineering that integrates electrical, mechanical, computer, and control system technologies together and is all governed by control algorithms. The precision, accuracy, and usability of a robot heavily rely on its motion control system. Figure 1 presents the Mechatronics architecture of a robot. The control system execution server runs the control algorithms. Actuators attached between links provide motions and sensors act as feedback devices. The sensor interfacing circuit is used for removing noise and amplifying the signals. Power amplifiers are used to control high-power actuators based on the output command from the control system execution server.

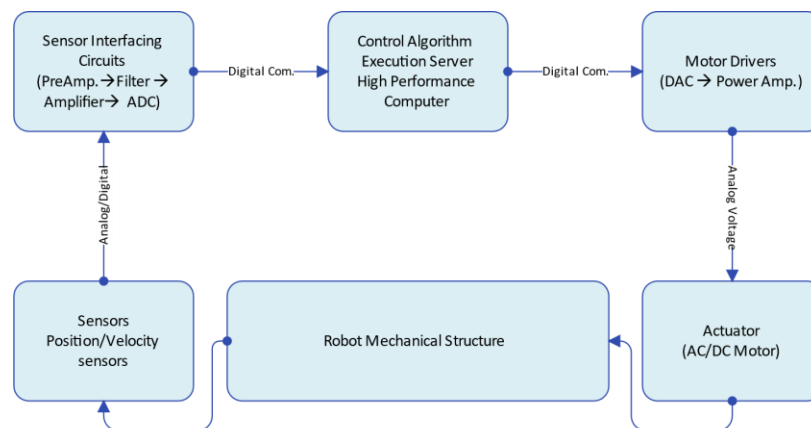


Figure 1 Mechatronics architecture of a robot

Model-based control is popular for robot control application that uses the kinematic and dynamic model of the robot as part of the control algorithms. Two commonly employed techniques for deriving the dynamic equation of motion for robots are Newton-Euler's method and the Lagrange energy method [7]. Regardless of the method employed, the final dynamic equation of motion remains identical. Robot dynamics are nonlinear. The major sources of nonlinearities are configuration dependant mass/inertia,

gravity, Coriolis and centrifugal forces, and joint friction forces. The dynamic model facilitates the separation of these nonlinearity sources from the overall dynamic model. The internal architecture of robot dynamics is shown in Figure 4.

The dynamic model of the robot comprises of configuration dependant mass, gravity, Coriolis-centrifugal forces, and friction matrices. During the linearization process, the gravity, Coriolis and centrifugal forces, and joint friction forces are computed separately and feedback to the physical robot to remove nonlinearities associated with them. Robot input is multiplied by the mass matrix to remove the nonlinearities associated with the position-dependent mass and inertia. Upon linearization, the angular acceleration of the robot joint becomes proportional to the applied torques, and the mass matrix acts as the proportional constant. Any linear control scheme can be employed to control robot dynamics. The whole process is a great example of a model-based control system. Figure 9 depicts the architecture of a model-based control system.

Numerous robot control methods are currently in use, including linear [8, 9], nonlinear [10], robust [11], optimal [9], and adaptive [12] control schemes. Upon analyzing the established control techniques [8-12], it has become evident that most of the available control schemes are model-based control. Different components of the robot's dynamic equation of motion are utilized for both linearization and control purposes.

For robots with higher degrees of freedom, the dynamics become intricate and computationally intensive. Most of the robot control algorithms are based on joint torque control, which necessitates a higher sampling rate compared to position or velocity control schemes [8, 9, 11-15]. Completing the execution of robot dynamics within the specified sampling period demands substantial computational power. The mass, gravity, and Coriolis-centrifugal matrices of the dynamic equation of motion are sequentially structured, multicore CPU or GPU neither boosts the performance nor reduces the execution time. A trained neural network-based equivalent computationally lightweight parallel structured model facilitates to use CPU and GPU combindly to speed up the control algorithm execution.

Deep learning has emerged as a powerful technique for solving classification and prediction problems [16]. Deep learning technology is used extensively across various domains. Dragan et al. presented more details about different domains of the deep neural network [17]. Extensive research has been carried out on the utilization of neural networks for robot dynamic modeling and control. Some prominent works that used neural networks for robot control applications are discussed below.

Chen et al. [18] combined the iterative learning control with a neural network to improve the trajectory tracking performance of a multi-degrees of freedom industrial robot. Physical stimulations were applied

to identify the internal dynamics of the robot. To compensate for the robot's internal dynamics and time delay, a neural network-based inverse dynamic model was developed and added as a feed-forward gain.

Su et al. [19] employed a neural network-based controller to effectively control a single-link flexible manipulator. They developed two distinct neural networks with an adaptive mechanism to compensate for the nonlinearities and friction. Subsequently, a linear control scheme was used to govern the flexible manipulator. Additional scholarly investigations on neural network-assisted control of flexible link manipulators can be found in the following references [20-25].

Lin et al [26] developed a deep neural network to compensate for gravity and external disturbances. For gravity compensation, a feed-forward neural network was trained based on the dynamics of the system. In order to model the external disturbances, two distinct scenarios were considered: configuration-dependent disturbances and direction-dependent disturbances. A big neural network was developed to effectively reject these disturbances. For real-time implementation, the researchers employed the knowledge distillation technique to condense the big neural network.

Mukhopadhyay et al. [27] modeled a robot's dynamic using a neural network. They used the robot's sensor data for training recurrent neural networks. They conducted a comparative study between three different types of recurrent neural networks: Simple Recurrent Neural Network (SRNN), Long Short-Term Memory (LSTM), and Gated Recurrent Unit (GRU) and discussed different aspects of selecting the appropriate Recurrent Neural Network for dynamic modeling. Similarly, Liu et al [28] used LSTM to develop an inverse dynamics model of a robot. Step input function was used as the input trajectories and Newton Euler's analytical model was used for calculating the output torque. By pairing input and output data, they trained the developed neural network.

Liang et al. [29] modeled robot dynamics by trained deep-learning neural networks. They used real-time physical data. They applied physical stimulation to the robot and used input-output data set for online training.

Panwar et al. [30] used a neural network to generate bipedal robot trajectories that emulate human-like movements. They incorporated upper body movements to ensure the overall stability of the robot's body.

Narendra et al. [31] demonstrated the applicability of neural networks in identifying and controlling nonlinear dynamics. They concluded that a multilayer recurrent neural network with a specific configuration can effectively be employed for both identification and control tasks of nonlinear dynamical systems.

Polydoros et al. [32] developed a real-time deep-learning network specifically designed for robotic applications. This network demonstrated the ability to effectively learn from noisy data and exhibited rapid convergence. The researchers conducted simulations that showcased the superiority of the algorithms in various robotic applications.

The application of neural networks in developing adaptive controllers for robots has gained widespread popularity, as evidenced by numerous studies [33-37].

By analyzing the above-mentioned literature, it has been noticed that neural network has been extensively used for robot dynamic modeling and control application, but a systematic way to produce physics-based data for inverse modeling of multi degrees of freedom robotics manipulator along with deep neural network-based dynamic controller is absent, which provides us an opportunity to contribute to this field.

The contribution of this article is to: a) Present a technique to generate physics-governed training data for the machine learning based multi degrees of freedom robot control applications b) Develop a deep neural network-based hybrid multi-degrees of freedom serial link robot controller, which is computationally lightweight and allows CPU, GPU combined architecture for computation. Provides high trajectory tracking performances similar to other conventional nonlinear control techniques.

The whole article can be divided into 8 sections. Section 1 introduced readers to the state of the art of different control schemes with a focus on neural network-based robot control techniques, problem definition, and proposed solutions. Section 2 describes the dynamic modeling of the human lower extremity exoskeleton robot. Section 3 explains the computed torque control technique. Section 4 presents dynamic simulation, data collection, defining the architecture of deep neural networks, its training, and validation. Section 5 presents the development of hybrid control algorithms using the deep neural network and a PD controller, which is followed by the stability analysis of the proposed controller. Section 6 presents the simulation results of the developed hybrid controller. Section 7 shows the robustness of the developed controller on parameter variations using ANOVA. Finally, section 8 presents the comparative studies between the developed hybrid controller and the Computed Torque Controller, Model Reference Computed Torque Controller, Sliding Mode Controller, Adaptive controller, and Linear Quadratic Regulator while keeping the same robot dynamics.

## **2. Dynamic Modeling of the Exoskeleton Robot**

The modified DH parameter approach (Figure 2) was used to allocate link frames to individual degrees of freedom and the resultant DH parameter table (Table 1) was constructed. By substituting the value of the DH parameters in the general form of the homogeneous transformation matrix shown in Eqn. (1), the individual transformation matrix was found (Eqn. (2)-(8)). The complete forward kinematics was

obtained by multiplying 7 transformation matrices together (Eqn. (9)). The forward kinematics specifies the end frame's position and orientation relative to the base frame.

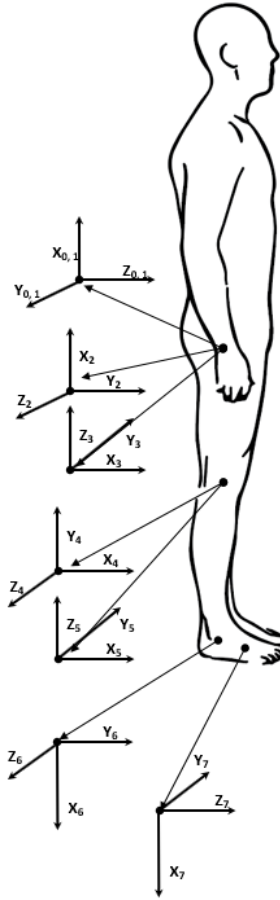


Figure 2 Link Frame assignment based on modified D-H parameter

Table 1: Human lower extremity DH parameters

Joint (i)	Joint name	Joint variable	Link offset	Link length	Link twist	
		$\theta_i$	$d_i$	$a_{i-1}$	$\alpha_{i-1}$	
1.	Abduction/Adduction	$\theta_1$	0	0	0	
2.	Hip	Flexion/Extension	$\theta_2 - \frac{\pi}{2}$	0	0	$-\frac{\pi}{2}$
3.		Internal/External rotation	$\theta_3$	$-l_1$	0	$-\frac{\pi}{2}$
4.	Knee	Flexion/Extension	$\theta_4$	0	0	$\frac{\pi}{2}$
5.		Internal rotation	$\theta_5$	$-l_2$	0	$-\frac{\pi}{2}$

6.	Ankle	Dorsiflexion/Plantarflexion	$\theta_6 - \frac{\pi}{2}$	0	0	$\frac{\pi}{2}$
7.		Pronation/Supination	$\theta_7$	0	$a_1$	$-\frac{\pi}{2}$

$${}^i_{i-1}T = \begin{bmatrix} \cos\theta_i & -\sin\theta_i & 0 & \alpha_{i-1} \\ \sin\theta_i \cos\alpha_{i-1} & \cos\theta_i \cos\alpha_{i-1} & -\sin\alpha_{i-1} & -\sin\alpha_{i-1} d_i \\ \sin\theta_i \sin\alpha_{i-1} & \cos\theta_i \sin\alpha_{i-1} & \cos\alpha_{i-1} & \cos\alpha_{i-1} d_i \\ 0 & 0 & 0 & 1 \end{bmatrix} \quad (1)$$

$${}^0T_1 = \begin{bmatrix} \cos(\theta_1) & -\sin(\theta_1) & 0 & 0 \\ \sin(\theta_1) & \cos(\theta_1) & 0 & 0 \\ 0 & 0 & 1 & 0 \\ 0 & 0 & 0 & 1 \end{bmatrix} \quad (2)$$

$${}^1T_2 = \begin{bmatrix} \sin(\theta_2) & \cos(\theta_2) & 0 & 0 \\ 0 & 0 & 0 & 0 \\ \cos(\theta_2) & -\sin(\theta_2) & 1 & 0 \\ 0 & 0 & 0 & 1 \end{bmatrix} \quad (3)$$

$${}^2T_3 = \begin{bmatrix} \cos(\theta_3) & -\sin(\theta_3) & 0 & 0 \\ 0 & 0 & 0 & -l_1 \\ -\sin(\theta_3) & -\cos(\theta_3) & 1 & 0 \\ 0 & 0 & 0 & 1 \end{bmatrix} \quad (4)$$

$${}^3T_4 = \begin{bmatrix} \cos(\theta_4) & -\sin(\theta_4) & 0 & 0 \\ 0 & 0 & -1 & 0 \\ \sin(\theta_4) & \cos(\theta_4) & 0 & 0 \\ 0 & 0 & 0 & 1 \end{bmatrix} \quad (5)$$

$${}^4T_5 = \begin{bmatrix} \cos(\theta_5) & -\sin(\theta_5) & 0 & 0 \\ 0 & 0 & 1 & -l_2 \\ -\sin(\theta_5) & -\cos(\theta_5) & 0 & 0 \\ 0 & 0 & 0 & 1 \end{bmatrix} \quad (6)$$

$${}^5T_6 = \begin{bmatrix} \sin(\theta_6) & \cos(\theta_6) & 0 & 0 \\ 0 & 0 & -1 & 0 \\ -\cos(\theta_6) & \sin(\theta_6) & 0 & 0 \\ 0 & 0 & 0 & 1 \end{bmatrix} \quad (7)$$

$${}^6T_7 = \begin{bmatrix} \cos(\theta_7) & -\sin(\theta_7) & 0 & a_1 \\ 0 & 0 & 1 & 0 \\ -\sin(\theta_7) & -\cos(\theta_7) & 0 & 0 \\ 0 & 0 & 0 & 1 \end{bmatrix} \quad (8)$$

$${}^0_7T = \begin{bmatrix} 0 & 1 & 2 & 3 & 4 & 5 & 6 \\ 1 & T_2 & T_3 & T_4 & T_5 & T_6 & T_7 \end{bmatrix} \quad (9)$$

Lagrange's energy method is a compelling technique to capture the dynamics of a rigid body. At any given moment the potential energy of a rigid body depends on its position Eqn. (10)-(11) and the kinetic energy

of the rigid body depends on the velocity Eqn. (12)-(13). After computing the total energy, using the Lagrange method (equation (14)) the dynamic equation of motion was developed.

$$u_i = -m_i \cdot {}^0g^T \cdot {}^0P_{ci} + u_{ref} \quad (10)$$

$$u = \sum_{i=1}^n u_i \quad (11)$$

$$k_i = \left[ \frac{1}{2} m_i \cdot v_{ci}^T \cdot v_{ci} + \frac{1}{2} {}^i\omega_{ci}^T \cdot {}^{ci}I_i \cdot \omega_{ci} \right] \quad (12)$$

In Eq. (10),  $m_i$  is the mass of the link,  $g$  is the gravitational acceleration, and  ${}^0P_{ci}$  is the location of the center of mass of the link with respect to the reference ground. In Eqn. (11),  $n$  is the total number of links. In Eqn. (12),  $m_i$  present the mass of the link,  $v_{ci}$  and  $\omega_{ci}$  express the linear and angular velocity of the link at the link's center of mass and  $I_i$  is the link's moment of inertia at its center of mass.

$$k = \sum_{i=1}^n k_i \quad (13)$$

$$\tau_i = \left[ \frac{d}{dt} \frac{\delta k}{\delta \dot{\theta}_i} - \frac{\delta k}{\delta \theta_i} + \frac{\delta u}{\delta \theta_i} \right] \quad (14)$$

The anthropometric parameters that were used for developing the robot dynamics equation of motion are given in Eqn. (15)-(35),

$$B_d = 0.6905 + 0.0297C \frac{lb}{ft^3}, \text{ where } C = HW^{-\frac{1}{3}}, \quad (15)$$

In Equation (15),  $B_d$  is the body density ( $lbs/ft^3$ ),  $H$  is the height of the subject ( $inch$ ),  $W$  is the body weight of the subject ( $lbs$ ). Thigh, shank, and foot densities determined by Eqn. (16) to Eqn. (18)

$$T_d = 1.035 + 0.814 * B_d \frac{lb}{ft^3} \quad (16)$$

$$S_d = 1.065 + B_d \frac{lb}{ft^3} \quad (17)$$

$$F_d = 1.071 + B_d \frac{lb}{ft^3} \quad (18)$$

In Eqns. (16)-(18),  $T_d$  is the thigh density,  $S_d$  is the shank density and  $F_d$  is the foot density. The whole-body volume ( $B_v$ ) was calculated using body weight and body density (Eqn. (19)),

$$B_v = \frac{W}{B_d} ft^3 \quad (19)$$

The volume of the thigh, shank, and foot were calculated as follows (Eqn. (20) to Eqn. (22))

$$T_v = 0.0922 * B_v ft^3 \quad (20)$$

$$S_v = 0.0464 * B_v ft^3 \quad (21)$$

$$F_v = 0.0124 * B_v ft^3 \quad (22)$$

The weights of the thigh, shank, and foot were calculated by the Eqns. (23)-(25)

$$T_m = T_v * T_d lbs \quad (23)$$

$$S_m = S_v * S_d lbs \quad (24)$$

$$F_m = F_v * F_d lbs \quad (25)$$

The length of the thigh ( $T_l$ ), shank ( $S_l$ ), foot ( $F_l$ ) and ankle to the lower face of the foot ( $A_g$ ) were calculated by Eqns. (26)-(29),

$$T_l = 0.245 * H inch, \quad (26)$$

$$S_l = 0.285 * H inch, \quad (27)$$

$$F_l = 0.152 * H inch, \quad (28)$$

$$A_g = 0.043 * H inch \quad (29)$$

The locations of the center of the mass from the proximal joint (for thigh ( $T_{cm}$ ), shank ( $S_{cm}$ ), foot ( $F_{cm}$ )) are given by Eqns. (30) - (32)

$$T_{cm} = 0.41 * T_l inch, \quad (30)$$

$$S_{cm} = 0.393 * S_l inch, \quad (31)$$

$$F_{cm} = 0.445 * F_l inch \quad (32)$$

The empirical equations for the inertial properties of the thigh  $T_i$ , shank  $S_i$ , and foot  $F_i$  are given in Eqns (33) - (35),

$$T_i = \begin{bmatrix} T_m (0.124 * T_l)^2 & 0 & 0 \\ 0 & T_m (0.267 * T_l)^2 & 0 \\ 0 & 0 & T_m (0.267 * T_l)^2 \end{bmatrix} \quad (33)$$

$$S_i = \begin{bmatrix} S_m (0.281 * S_l)^2 & 0 & 0 \\ 0 & S_m (0.114 * S_l)^2 & 0 \\ 0 & 0 & S_m (0.275 * S_l)^2 \end{bmatrix} \quad (34)$$

$$F_i = \begin{bmatrix} F_m (0.124 * F_l)^2 & 0 & 0 \\ 0 & F_m (0.245 * F_l)^2 & 0 \\ 0 & 0 & F_m (0.257 * F_l)^2 \end{bmatrix} \quad (35)$$

Eqn. (15)-(35) were incorporated into the dynamic equation of motion of the robot.

The robot's dynamic equation of motion ((14) can be rewritten as Eqn. (36),

$$\tau_{Joint} = [M(\theta)\ddot{\theta} + V(\theta, \dot{\theta}) + G(\theta)] \quad (36)$$

A 7 DOF human lower extremity dynamic model was developed. In Eqn. (36),  $M(\theta)$  is the mass matrix which is a  $(7 \times 7)$  symmetric positive definite matrix,  $V(\theta, \dot{\theta})$ ,  $(7 \times 1)$  is the Coriolis and the centripetal term, and the gravitational term is represented by  $G(\theta)$ ,  $(7 \times 1)$  matrix.  $\tau_{Joint}$ ,  $(7 \times 1)$  presents the joints torque requirements.

The robot dynamic equation of motion Eqn. (36) can be written as,

$$\ddot{\theta} = M(\theta)^{-1}[\tau_{Joint} - V(\theta, \dot{\theta}) - G(\theta)] \quad (37)$$

Figure 3 shows the architecture of an ideal robot dynamics (without considering joint friction).

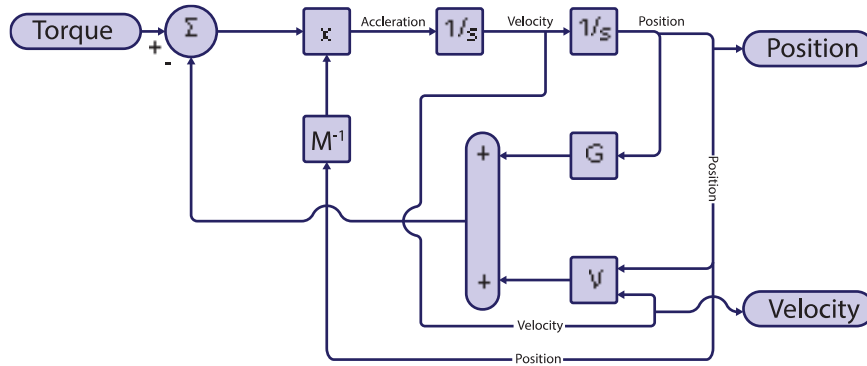


Figure 3 Internal architecture of the robot model

Naturally, friction is induced between two mechanical mating parts with relative motion. The robot dynamics grow more complex by incorporating joint friction torques.

$$\tau_{Joint} = [M(\theta)\ddot{\theta} + V(\theta, \dot{\theta}) + G(\theta) + \tau_{friction}] \quad (38)$$

Where,

$$\tau_{friction} = [f(\dot{\theta})] \quad (39)$$

Eqn. (37) can be rewritten as Eqn. (40)

$$\ddot{\theta} = M(\theta)^{-1}[\tau_{Joint} - V(\theta, \dot{\theta}) - G(\theta) - f(\dot{\theta})] \quad (40)$$

The robot dynamics with frictional disturbances are schematically depicted in Figure 4

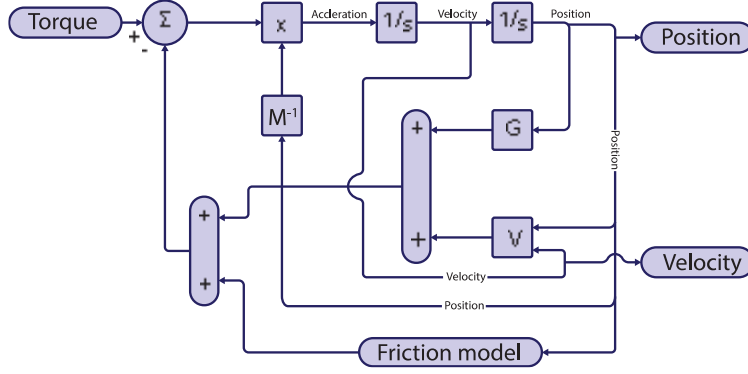


Figure 4 Internal architecture of the physical Robot model

The used friction model combined the Coulomb friction, the Viscous friction, and the Stribeck effect [38].

The Eqn. (41) to Eqn. (43) Approximate the joint friction torques:

$$T = \sqrt{(2e)}(T_{brk} - T_C) \cdot \exp\left(-\left(\frac{\omega}{\omega_{St}}\right)^2\right) \cdot \frac{\omega}{\omega_{St}} + T_C \cdot \tanh\left(\frac{\omega}{\omega_{Coul}}\right) + f\omega \quad (41)$$

$$\omega_{St} = \omega_{brk} \sqrt{2} \quad (42)$$

$$\omega_{Coul} = \frac{\omega_{brk}}{10} \quad (43)$$

Where,

$T$  represents the total friction

$T_C$  represents the Coulomb friction

$T_{brk}$  represents the breakaway friction torque: The Breakaway friction is defined as the sum of the Coulomb and Stribeck frictions in the vicinity of zero velocity.

$\omega_{brk}$  represents the breakaway friction velocity: The velocity at which the Stribeck friction is at its peak. At this point, the sum of the Stribeck and Coulomb friction is the Breakaway friction force.

$\omega_{St}$  represents the Stribeck velocity threshold

$\omega_{Coul}$  represents the Coulomb velocity threshold

$\omega$  represents the input angular velocity

$f$  is the coefficient of viscous friction: The coefficient of proportionality between the friction torque and the angular velocity. The parameter must have a positive value.

The simulation of the developed friction model is shown in Figure 5.

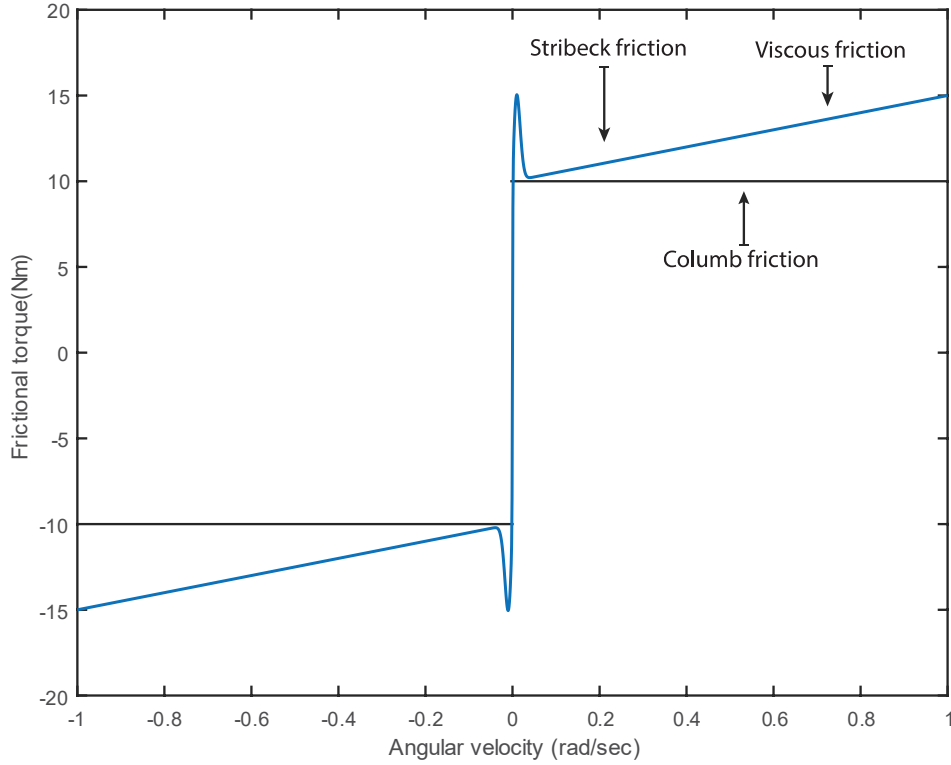


Figure 5 Friction model simulation

The parameters used for friction simulation are given below,

$$T_{Peak} = 100 \text{ Nm}, \omega = 100 \text{ rad/sec}, f = 5 \text{ Nm/(rad/sec)}, T_{Columb} = 0.1 * T_{Peak} \text{ Nm},$$

$$\omega_{brk} = 0.01 \text{ rad/sec}, T_{brk} = 0.15 * T_{Peak} \text{ Nm}$$

The following section will discuss the Computed Torque control scheme.

### 3. Computed Torque control

The computed torque control scheme calculates robot joints' trajectory tracking torque requirements by using robot inverse dynamics. The computed torque control system accomplishes two goals: linearize the nonlinear robot dynamics by providing the required torque to mitigate the effects of gravity and Coriolis-centrifugal force, remove the effects of position-dependant mass or inertia (Figure 6, linearization loop) and to deliver the controlled torque to track the robot input trajectories (Figure 6, control loop).

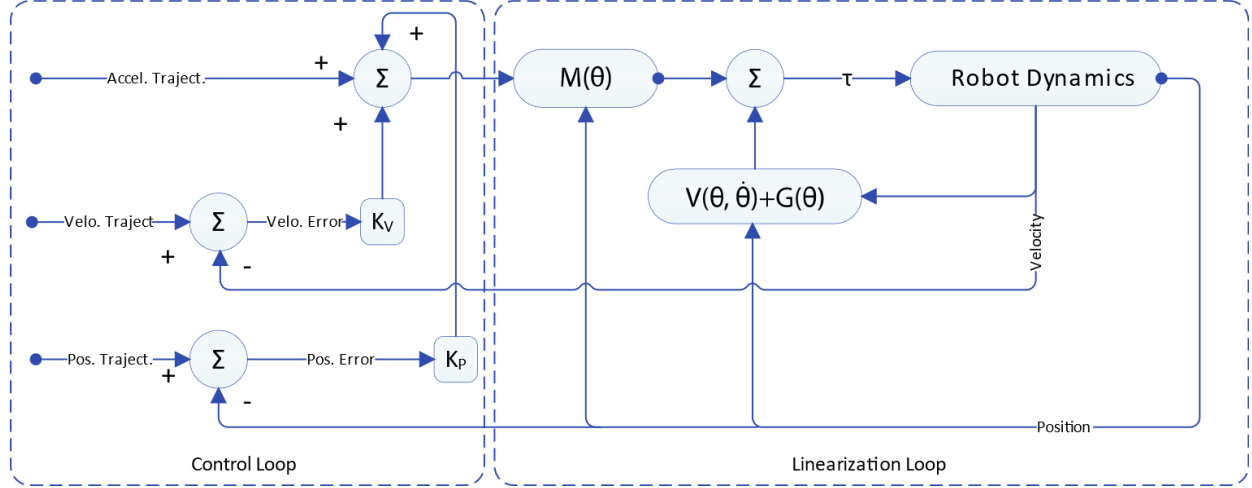


Figure 6 Computed torque control scheme

The main drawbacks of a computed torque controller are: an accurate dynamic model is impractical and the control algorithm involves execution of the whole robot dynamics on every sample time. It's a torque control scheme that requires a higher sampling rate compared to the position or velocity control scheme.

According to the robot computed torque control scheme, the input torque to the robot is given by Eq. (44),

$$\tau = M(\theta) [\ddot{\theta}_d + K_v(\dot{\theta}_d - \dot{\theta}) + K_p(\theta_d - \theta)] + V(\theta, \dot{\theta}) + G(\theta) \quad (44)$$

In Eqn. (44),  $\theta_d$ ,  $\dot{\theta}_d$  and  $\ddot{\theta}_d$  presents the robot's desired trajectories. The real position, velocity, and acceleration of the robot are represented by  $\theta$ ,  $\dot{\theta}$  and  $\ddot{\theta}$ .  $K_p, K_v$  are the positive definite gain matrices that act as the PD controller gain.  $M(\theta)$  presents the robot mass matrix,  $V(\theta, \dot{\theta})$  presents the Coriolis and centrifugal force and  $G(\theta)$  is the gravitational term of the robot dynamics.

#### 4. Dynamic modeling using Deep Neural Network

A neural network is a collection of interconnected neurons. A subdivision of neural networks with more than three layers is known as a Deep neural network (DNN) [39]. They are increasingly used as a modeling framework for neural computations in the primate brain [40]. The main advantage of DNN is that they can learn more abstract features than shallow neural networks [41]. DNNs can model complex non-linear relationships efficiently [42]. Due to their increased layer count, they may learn more intricate representations of the input data [41]. In addition, Deep neural networks can be used to solve issues that are challenging or impossible for conventional machine learning techniques to handle [43]. Due to the presence of extra layers, the computational load increases in DNNs. However, the advantages of employing deep neural networks generally outweigh this burden[39]. Deep neural network possesses

parallel structure, and multicore CPU/GPU or DSP can execute the control algorithms fast compare to the conventional model-based control algorithms [44].

Supervised learning uses labeled training data to teach a model to predict output from unseen data. Multi-layer neural network supervised learning process can be explained with the help of forward and backward propagation.

The steps and terminologies in the neural network forward propagation process are as follows:

1. **Input Layer:** The input layer of the neural network receives the input, which is typically a vector representing the features of the data point. In this research robot's input trajectories, user weight, and height were considered as the input of the developed deep neural network. A total of 23 inputs were considered.
2. **Hidden Layers:** Among the input and output layers one or more hidden layers exist. Each hidden layer consists of multiple neurons or nodes. Each node in a layer is connected to all nodes in the previous layer and all nodes in the subsequent layer. There are 3 hidden layers were used for the developed deep neural network. The first hidden layer consists of 21 neurons, the second hidden layer consists of 14 neurons and the third hidden layer consists of 7 neurons.
3. **Weighted Sum:** The inputs from the previous layers are multiplied by the corresponding weights in each neuron. By adding the products of the inputs and their corresponding weights and bias, the weighted total of these inputs is obtained.
4. **Activation Function:** After computing the weighted sum, an activation function is used to introduce non-linearity into the model. Typical activation functions are sigmoid, ReLU, tanh, and softmax. Based on its input, the activation function calculates the neuron's output value. In our developed deep neural network Tan hyperbolic activation function was used for the hidden layers and pure linear activation was used at the output layer. Figure 7 shows the Hyperbolic tangent and pure linear activation functions.

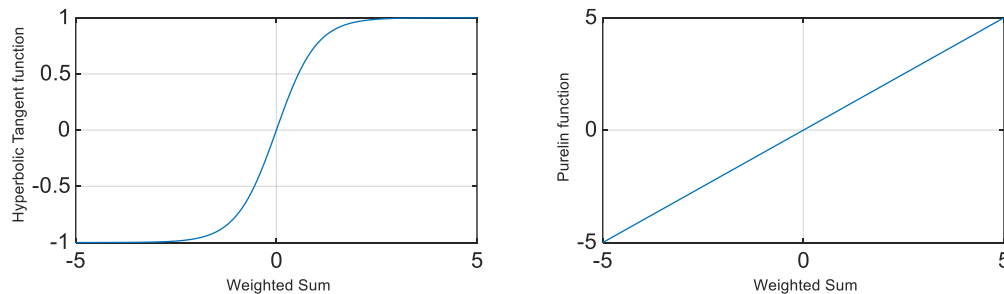


Figure 7 Hyperbolic tangent and pure linear activation functions

5. **Output Layer:** The output layer receives the output of the activations from the last hidden layer. Based on the requirements, the output layer may contain one or multiple neurons. The developed deep neural network has a total of 7 neurons at the output layer. Each neuron in the output layer represents a specific class or predicts a numerical value. In our case, the neurons at the output layer deliver predicted torques.
6. **Output Calculation:** The output layer calculates the final output based on the activations it receives. In a regression problem, the output layer delivers continuous numerical value.

After completing the forward propagation backward propagation process starts in supervised learning:

1. **Loss Calculation:** Backpropagation starts with the calculation of the loss or error between the network's anticipated output and its actual output for a certain training example. The choice of loss function depends on the application, for instance, mean squared error (MSE) for regression problems or cross-entropy loss for classification problems. As the developed deep neural network is solving a regression problem, MSE loss function was used to assess the errors.
2. **Output Layer Gradient:** After determining the loss, the next step is to assess the relationship between the loss and the activations in the output layer. The gradient of the loss function with respect to the activations of the output layer neurons is calculated to obtain this. The specific form of the gradient calculation depends on the chosen loss function.
3. **Backpropagation through Layers:** Once the gradient at the output layer is determined, it is propagated backward through the network. The goal is to calculate the gradients of the loss function with respect to the weights and biases of each layer in the network.
4. **Gradient Calculation:** In every layer, the gradients of the loss function with respect to the weights and biases are calculated using the chain rule of calculus. The gradient at a particular layer depends on the gradients in the subsequent layer, weighted by the corresponding weights connecting the layers.
5. **Weight Update:** After computing the gradients of the loss function with respect to the weights and biases, the weights are updated to minimize the loss. This is typically done using an optimization algorithm, such as gradient descent or one of its variants. The update rule involves subtracting a fraction of the gradient from the current weight, multiplied by the learning rate, which determines the step size of the update. In the developed deep neural network, Levenberg-Marquardt was used for updating neurons' weight and bias.
6. **Iterative Process:** Both forward and backward propagations are repeated for each training instance in the dataset. This iterative process of forward propagation, loss calculation, and backward propagation allows the model to adjust its weights and biases, gradually improving

its ability to make accurate predictions on unseen data. Figure 8 depicts the Multi-layer Neural network training process.

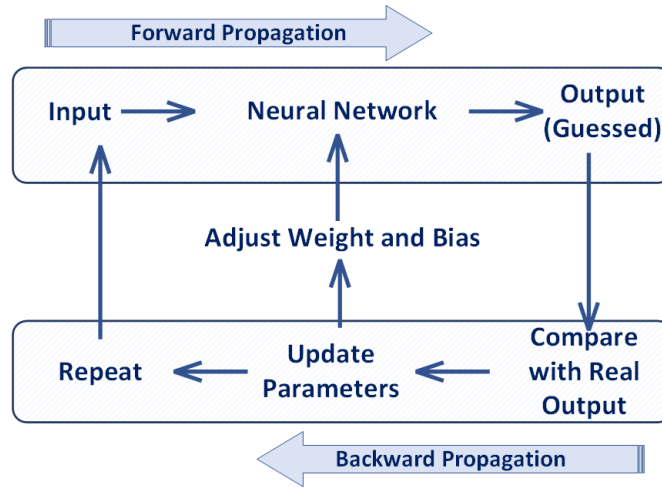


Figure 8 Multi-layer Neural network training process

When designing the structure of the deep neural network the main objectives were to maximize the prediction performance, minimize overfitting and alleviate the computational burden on the physical controller by reducing the network's size. The developed multi-layer neural network [45] architecture is shown in Figure 9. Different neural network structure were tested, the structure shown in Figure 9 gave the optimum performance. The constructed deep neural network consists of a total of 49 ( $L_1 \times 21, L_2 \times 14, L_3 \times 7, L_4 \times 7$ ) neurons, that are distributed across three hidden layers and one output layer. Instead of using a single hidden layer, multiple hidden layers were used to train more abstract features, reduce overfitting and enhance generalization. The developed network comprises a total of 224 weight elements (including neuron biases and weights). Tan-Sigmoid activation functions (hyperbolic tangent) were used in the hidden layers, while the linear activation functions (pure linear) were used in the output layer. During the construction of the neural network, various activation functions were tested for the hidden layers, the Tan-Sigmoid activation function demonstrated superior performance in terms of

both prediction accuracy and mitigating overfitting compared to alternative functions. It has been observed that adding an extra neuron in any layer or adding a new layer results in overfitting.

The Matlab `feedforwardnet(hiddenSizes, trainFcn)` command is used to construct the neural network [46]. Levenberg-Marquardt optimization function was used for updating the neuron’s weights and biases during backward propagation [47, 48]

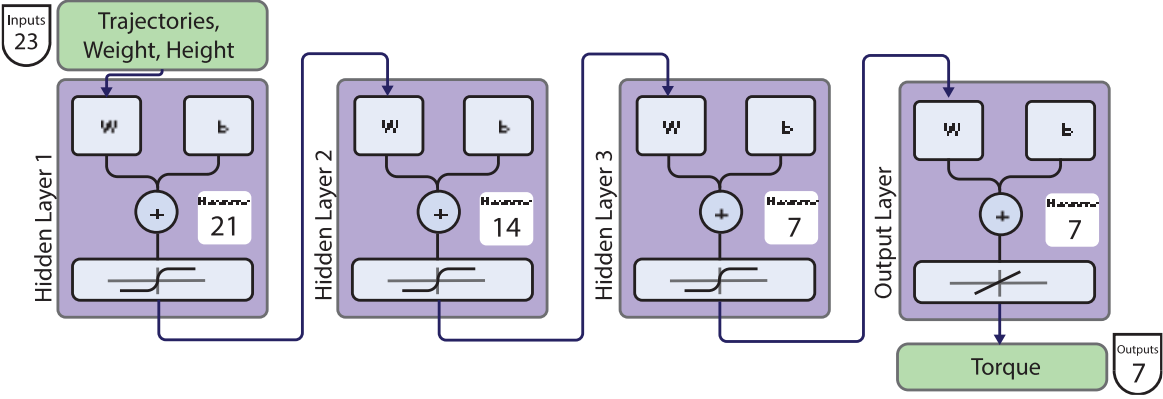


Figure 9 Architecture of the developed deep neural network

For training the developed neural network, two sets of data were generated. The first set was for the sequential joint movements: where seven joints moved successively, and the second set was for the simultaneous joint movements: when all the joints started moving together. Training Data were produced by hierarchical combinations of robot joint positions, velocities and accelerations, and subjects’ height and weight. The training data generation hierarchy is illustrated in Figure 11.

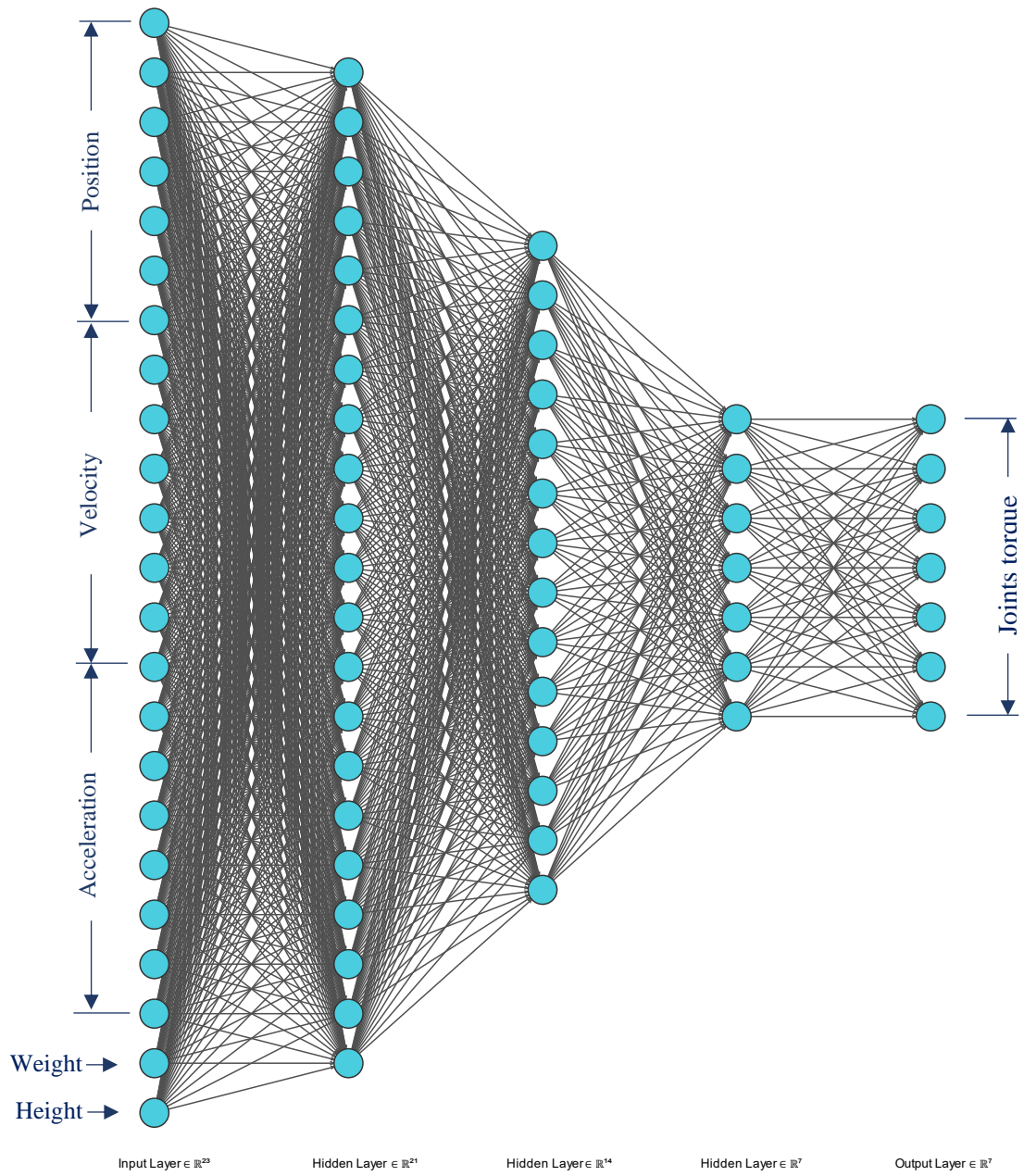


Figure 10 Developed deep neural network for joint torque estimation

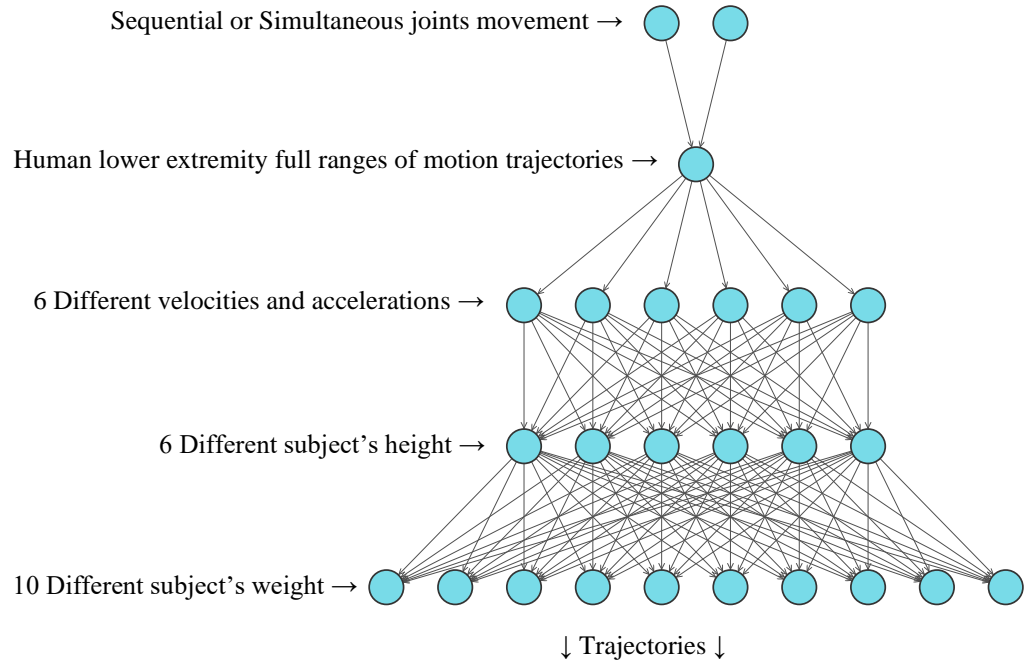


Figure 11 Hierarchical data generation schematic diagram

Seven joint positions, velocities, accelerations, subject's weight, and height obtained from different combinations were used as input to the computed torque controller-based dynamic simulation, and the outputs of the computed torque controller (7 joints torques) were logged for use as the training data. Figure 12 shows the schematics diagram of the computed torque controller-based dynamic simulation. The purple color highlighted the input of the simulation, and the green color presented the outputs.

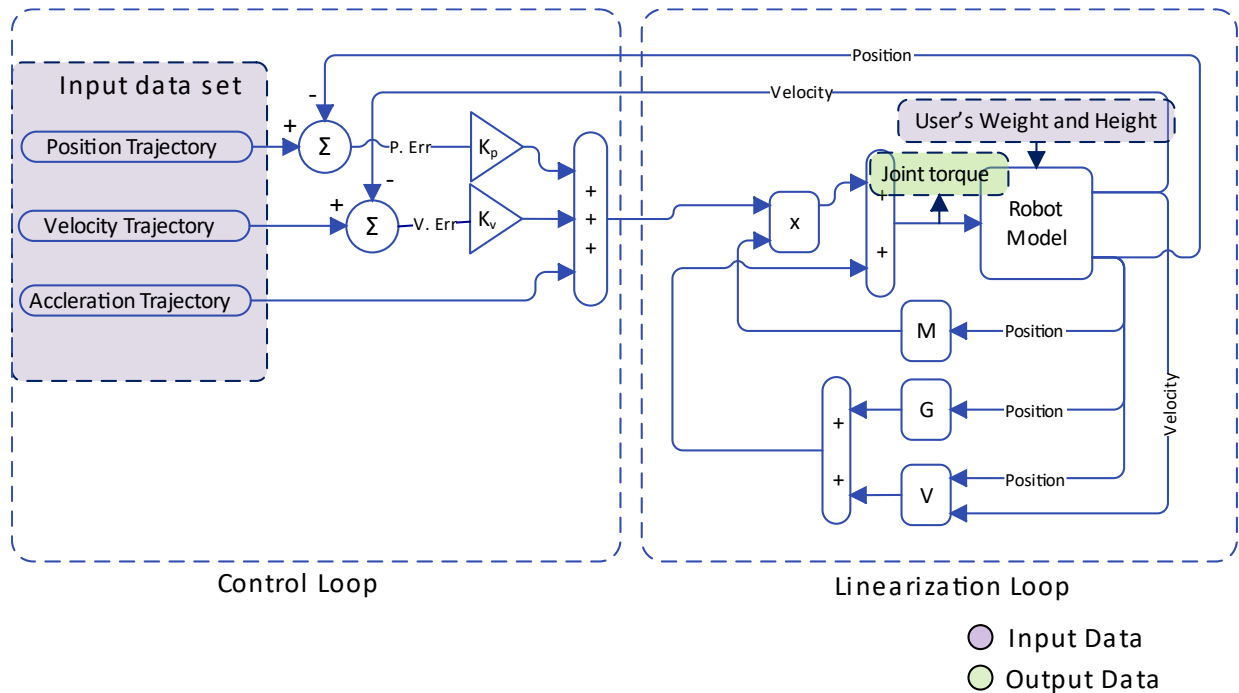


Figure 12 Input and Output data tracing locations in the simulation

Simulations were run for both sequential joint movements and simultaneous joint movements. A total of 43560880 sets of data were produced. Server computer with Intel Xeon processor 32 cores and 48 GB of memories can't handle this big amount of data. Collected data were down-sampled by a factor of 10 to reduce the data size. Correlation analyses of the data were performed to select the important features and reduce the input size. It has been noticed that input trajectories, weight, and height have a good correlation with the output torques, as a result, all inputs were considered. For the training, the neural network at a total of 4356088 sets of data was used. Each data set consists of 23 inputs (7 joints' desired positions, 7 joints' velocities, 7 joints' accelerations, user's height and weight) and 7 outputs (7 joints torques).

For the generation of the input data set, human lower extremity full ranges of motion were considered. Figure 13 presents the full ranges of motion trajectories. The left-side figure shows the simultaneous joint movements and the right-side figure shows the sequential joint movements.

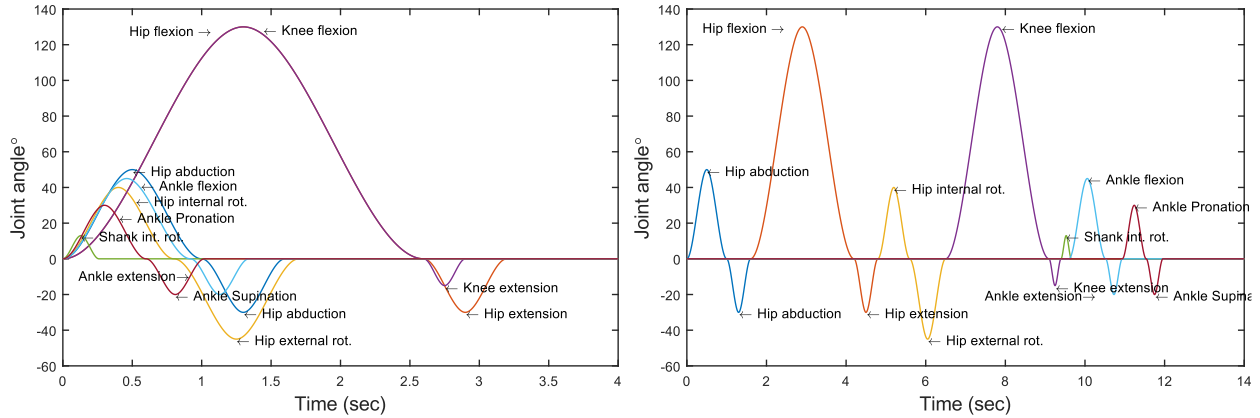


Figure 13 Simultaneous and sequential joint movements (constructed based on the human lower extremity's full ranges of motion [14])

For producing the deep neural network training data, the full ranges of motion position trajectories were run at different velocities with subjects' different heights and masses. Different configurations used for training data generation are given in Table 2.

Table 2 Different values of joints velocities, subject's weight and height used for training data generation

Joints velocity	10, 20, 30, 40, 50, 60, 70, 80, 90, 100 [deg/sec]
Subject's height	50, 55, 60, 70, 75 [inch]
Subject's weight	150, 160, 170, 180, 190, 200, 210, 220, 230, 240, 250 [lbs.]

The key role of the developed deep neural network is to estimate the joint's torque requirement based on the input trajectories and the subject's height and weight.

During training, 70% of the total data sets were used for network training, 15% for validation, and the remaining 15% used for testing. Training performances are quantified by the mean square error. Figure 14 presents the training, validation, and testing performance of the developed neural network.

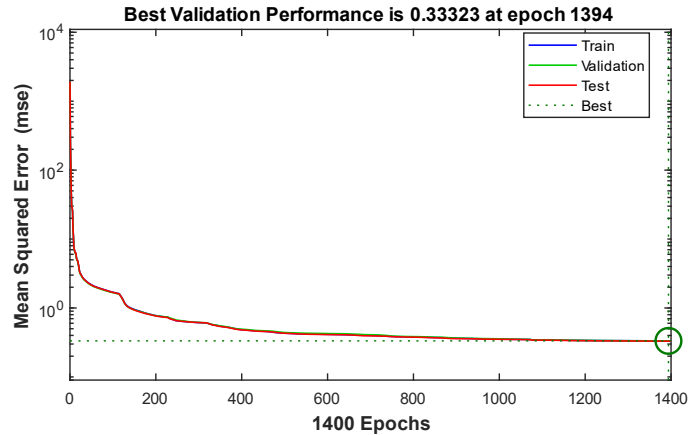


Figure 14 Training Neural network

### 5. Control algorithm based on the developed deep neural network

Figure 15 shows the architecture of the hybrid controller developed to maneuver the robot according to the input reference trajectories. Reference trajectories, user’s weight, and height were used as the input of the trained deep neural network. Seven joint torques were predicted by the deep neural network. The developed deep neural network provides the feed-forward gain to the controller. A PD controller was used inside the feedback loop to compensate for the prediction errors. The proportional gains ( $K_P$ ) 3000 and the derivative gains ( $K_V$ ) 250 were used for all joints of the PD controller.

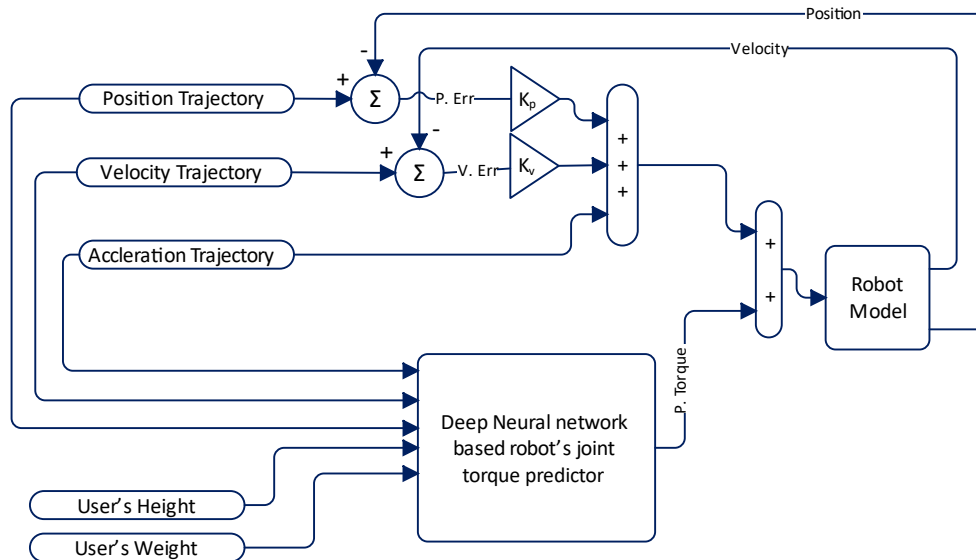


Figure 15 Control architecture of the Deep neural network-based robot controller

The prediction accuracy of the developed deep neural network depends on the the example data used for the training and the performance is specified by the testing, validation results. Training data were generated based on the analytical model of the exoskeleton robot, input trajectories and the user's weight and height. To ensure high performance of the developed Deep neural network an adequate amount of data based on different combinations were generated.

Higher prediction accuracy of the used deep neural network ensures better linearization, removing effects of gravity, Coriolis and Centrifugal force and neutralize the effects of position dependent mass matrix. The trained deep neural network acts as the feed-forward controller. The PD controller was employed as the feedback controller, which mainly removes the prediction errors. From Figure 16 shows the control architecture of the proposed controller.

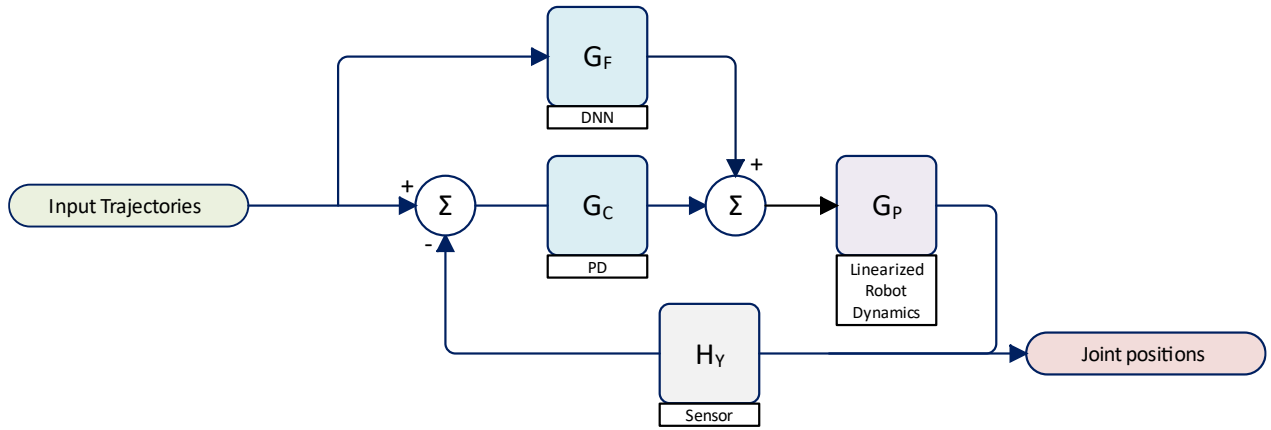


Figure 16 Control architecture of the hybrid controller

Figure 16 presents the control architecture of the developed hybrid controller. The transfer function between the input trajectories and the joint positions can be presented by

$$\frac{\text{Joint position}}{\text{Input trajectories}} = \frac{G_P G_F (1 + G_C G_P H_Y) + G_C G_P}{1 + G_C G_P H_Y} \quad (45)$$

In Eqn. (45) the characteristics equation is given by,

$$1 + G_C G_P H_Y = 0. \quad (46)$$

The stability of a given system depends on the characteristics equation. The characteristics equation is not a function of the feedforward gain  $G_F$ . Developed neural network removes nonlinearities caused by the gravitational force and Coriolis and centrifugal forces, it also cancels out the effect of the position dependent mass. After removing all the nonlinearities, the angular accelerations become proportional to the applied torques and the mass matrix acts as the unity gain proportional constant. The linearized decoupled model can be expressed by the Eqn. (47)

$$\tau = \ddot{\theta} \quad (47)$$

By applying the Laplace transform

$$\tau(s) = s^2\theta(s)$$

$$\frac{\theta(s)}{\tau(s)} = \frac{1}{s^2}$$

$$\text{So, } G_p(s) = \frac{\theta(s)}{\tau(s)} = \frac{1}{s^2}$$

PD controller can be written as,  $G_c(s) = K_p + K_d s$

Due to higher bandwidth and unity gain of the sensor, transfer function can be considered as 1

$$H_y = 1$$

By substituting the values of  $G_c, G_p, H_y$  into Eqn. (46). The characteristics equation become Eqn. (48)

$$s^2 + K_d s + K_p = 0 \quad (48)$$

The constructed Routh Hertz table based on the characteristic's equation (48) is given in Table 3

Table 3: Routh Hertz table

$s^2$	1	$K_p$
$s^1$	$K_d$	
$s^0$	$K_p$	

According to the Routh Hertz criteria, no sign change on the 1<sup>st</sup> column of the Routh table ensures stable system. Table 3 ensures that the developed control system will remain stable for any positive values of gain  $K_p$  and  $K_d$ .

The stability of the developed controller does not depend on the feed-forward gain  $G_F$ , which is provided by the deep neural network. The feed-forward gain either amplifies or attenuates the output signal, it would not be able to propagate the trajectory tracking errors. A well trained deep neural network along with a PD controller with a positive gain ensures the stability of the developed hybrid controller. The performance of the deep neural network can be ensured during the training and validation phase. The smaller value of the mean square error during network training and validation indicates better prediction performance.

## 6. Simulation results analysis

On this section we will simulate the human lower extremity dynamics using the developed deep neural network based hybrid controller and asses it's performances. Figure 17 to Figure 22 presents the trajectory tracking performances of the developed deep neural network-based hybrid controller in simultaneous joint movements. Figure 17 shows the trajectory tracking performance of all seven joints in

simultaneous movement. Both reference trajectories and the output trajectories are shown side by side on the figure. Due to the presence of very small amount of trajectory tracking errors, it is difficult to differentiate in between them. Figure 18 shows the trajectory tracking errors. The maximum amount of observed trajectory tracking errors were  $[0.26^\circ, 0.20^\circ, 0.20^\circ, 0.26^\circ, -0.14^\circ, -0.21^\circ, 0.19^\circ]$  for joint 1 to joint 7 respectively. From the simulation results, it has been shown that joint 4 experienced the maximum amount of trajectory tracking error ( $0.26^\circ$ ) followed by joint 1 and joint 6.

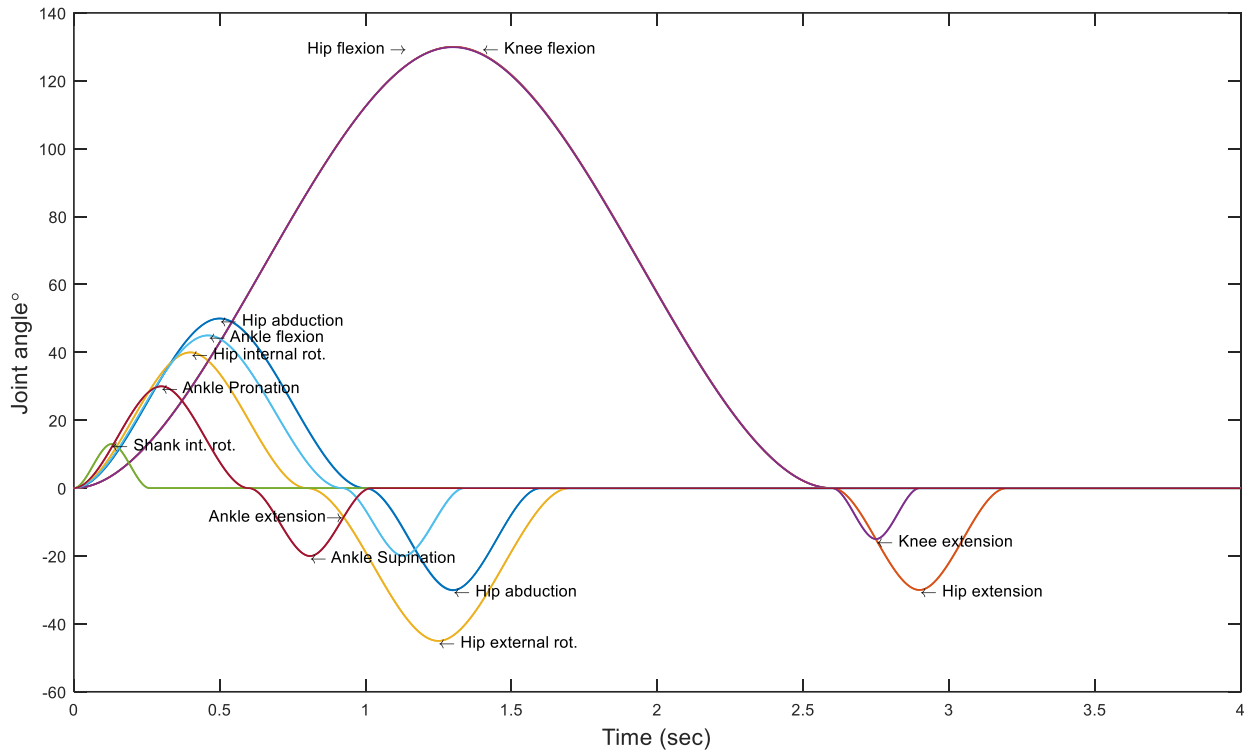


Figure 17 Trajectory tracking performance (Simultaneous joint movement)

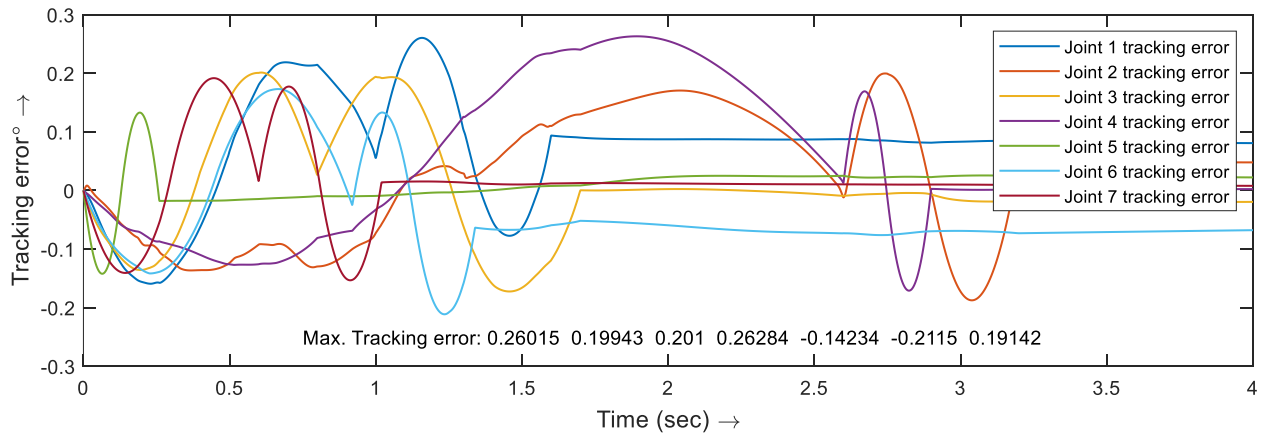


Figure 18 Trajectory tracking Error (Simultaneous joint movement)

Figure 19 shows the joint torque requirement for tracking the reference trajectories depicted in Figure 17. The left column of Figure 19 shows the total torque required for simultaneous trajectory tracking. The middle column of Figure 19 shows the predicted joints torques by the deep neural network and the right shows the contribution of the PD controller.

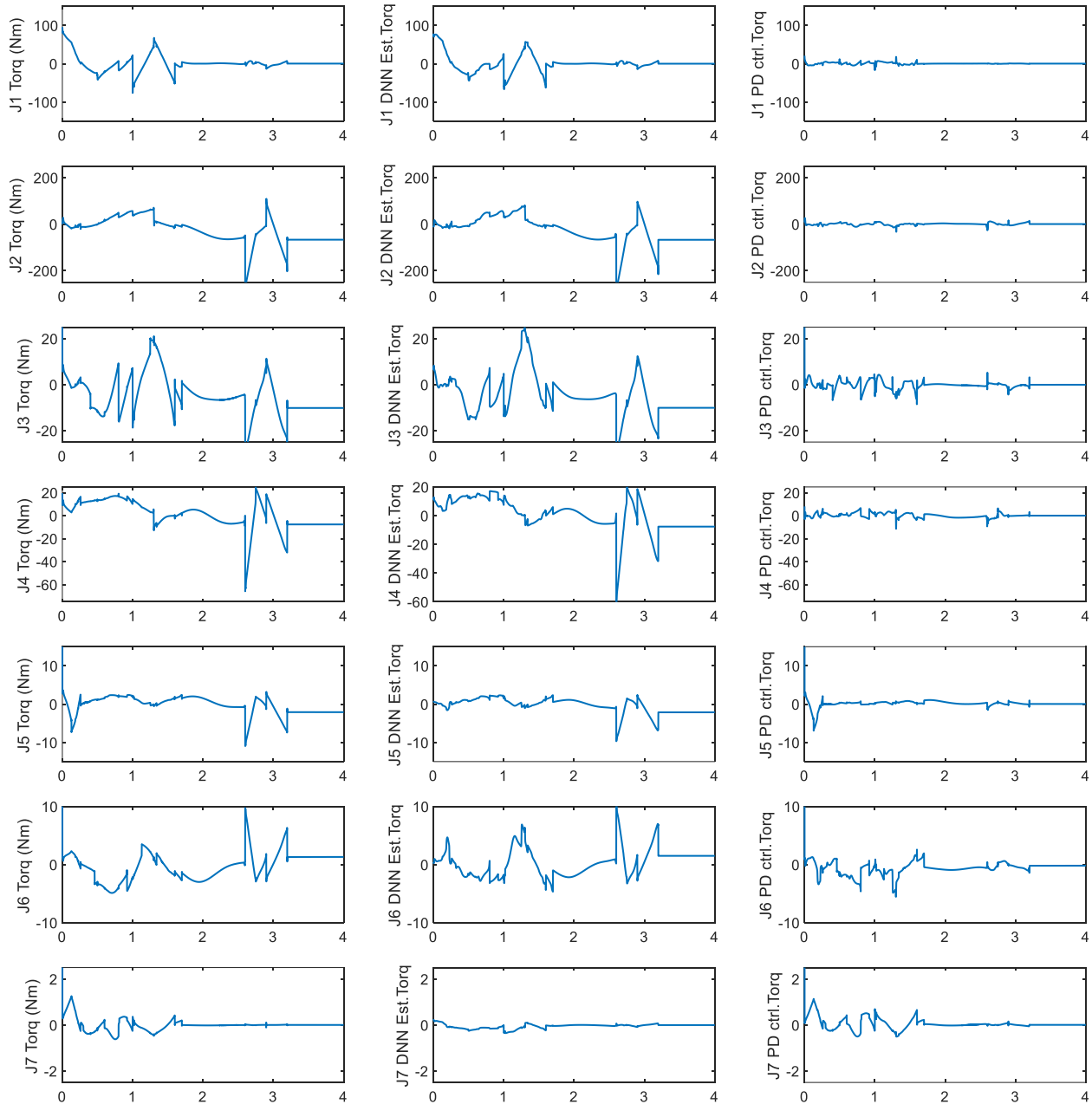


Figure 19 From the right: total Joint torque requirement for sequential joint movements, predicted torque, PD controller's contribution

From Figure 19, it is evident that the predicted torque closely matches the total required joint torque for all the joints except joint 7, with minimal contribution from the PD controller. For the 7<sup>th</sup> joint the PD

controller contributed little more than the predicted torque. Due to the black-box nature of the deep neural networks, it is very difficult to explain the inner mechanism. It was observed that the joint torque requirements for the seventh joint is significantly lower than other joints. Joint 7 dynamics was tried to capture by adding an extra neuron or an extra layer but by introducing an extra neuron or by adding an extra layer caused an overfitting problem.

The performance of the developed controller in sequential trajectory tracking is shown in Figure 20. As the output trajectories were very closely tracked the reference trajectories, it is difficult to separate the output trajectories from the reference trajectories (Figure 20). Figure 21 shows the observed trajectory tracking errors. The maximum amount of observed trajectory tracking errors were  $[-0.22^\circ, -0.26^\circ, -0.18^\circ, 0.25^\circ, -0.15^\circ, -0.19^\circ, -0.17^\circ]$ . Joint 2 experienced the maximum amount of trajectory tracking error ( $0.26^\circ$ ) followed by joint 4 and joint 1.

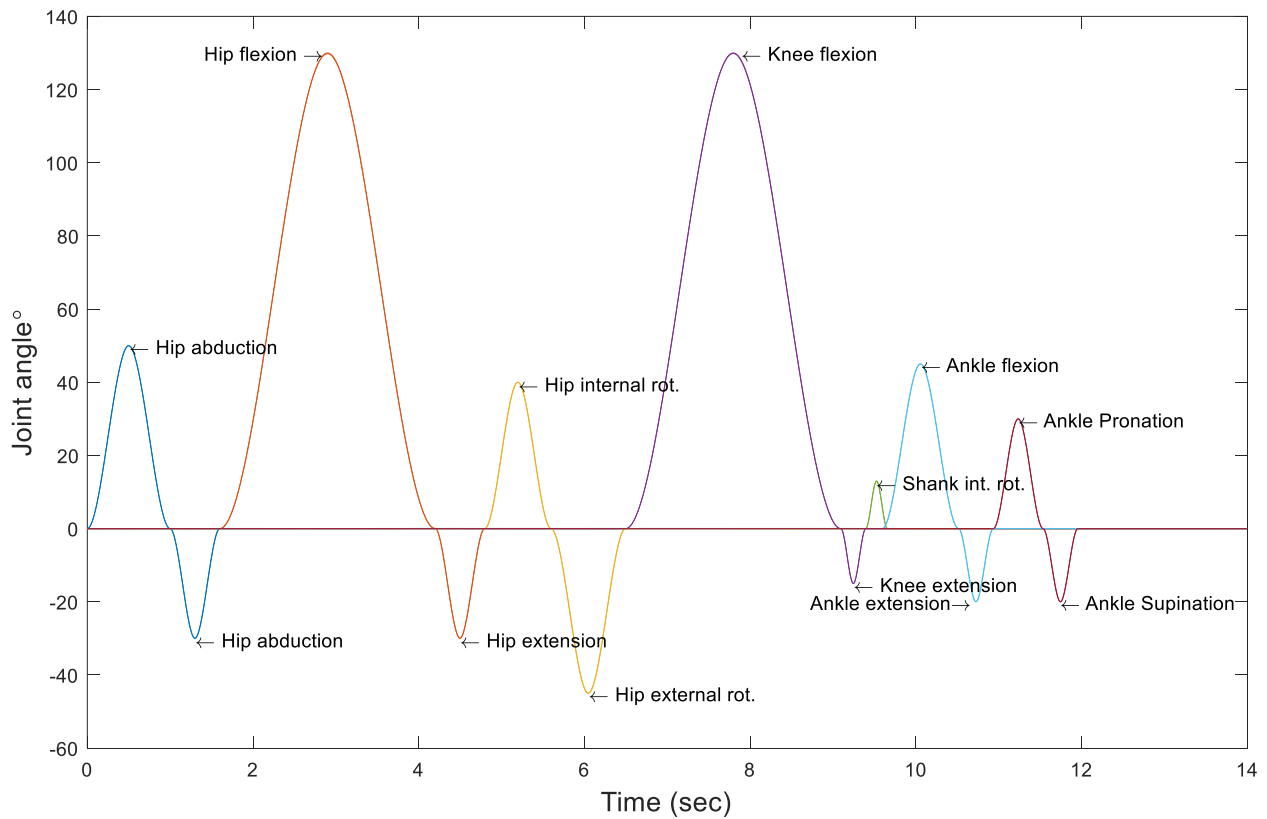


Figure 20 Trajectory tracking performance (Sequential joint movements)

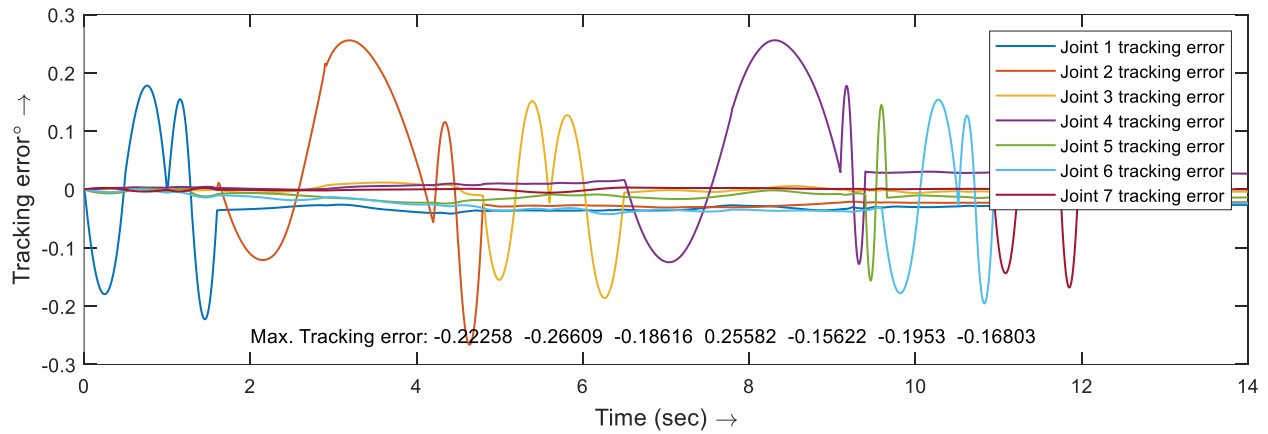


Figure 21 Trajectory tracking error (Sequential joint movements)

The joint torque distribution for the sequential trajectory tracking is shown in Figure 22. The left column shows the overall joint torque required for tracking the sequential movements. In the middle column of the Figure 22 shows the predicted torques by the deep neural network. On the right column, the contribution of the PD controller is depicted. Similar to the simultaneous joint movements, the maximum amount of prediction errors was observed on joint 7. From joint 1 to joint 6 the deep neural network predicted torques were very closely aligned to the total joint torque requirements.

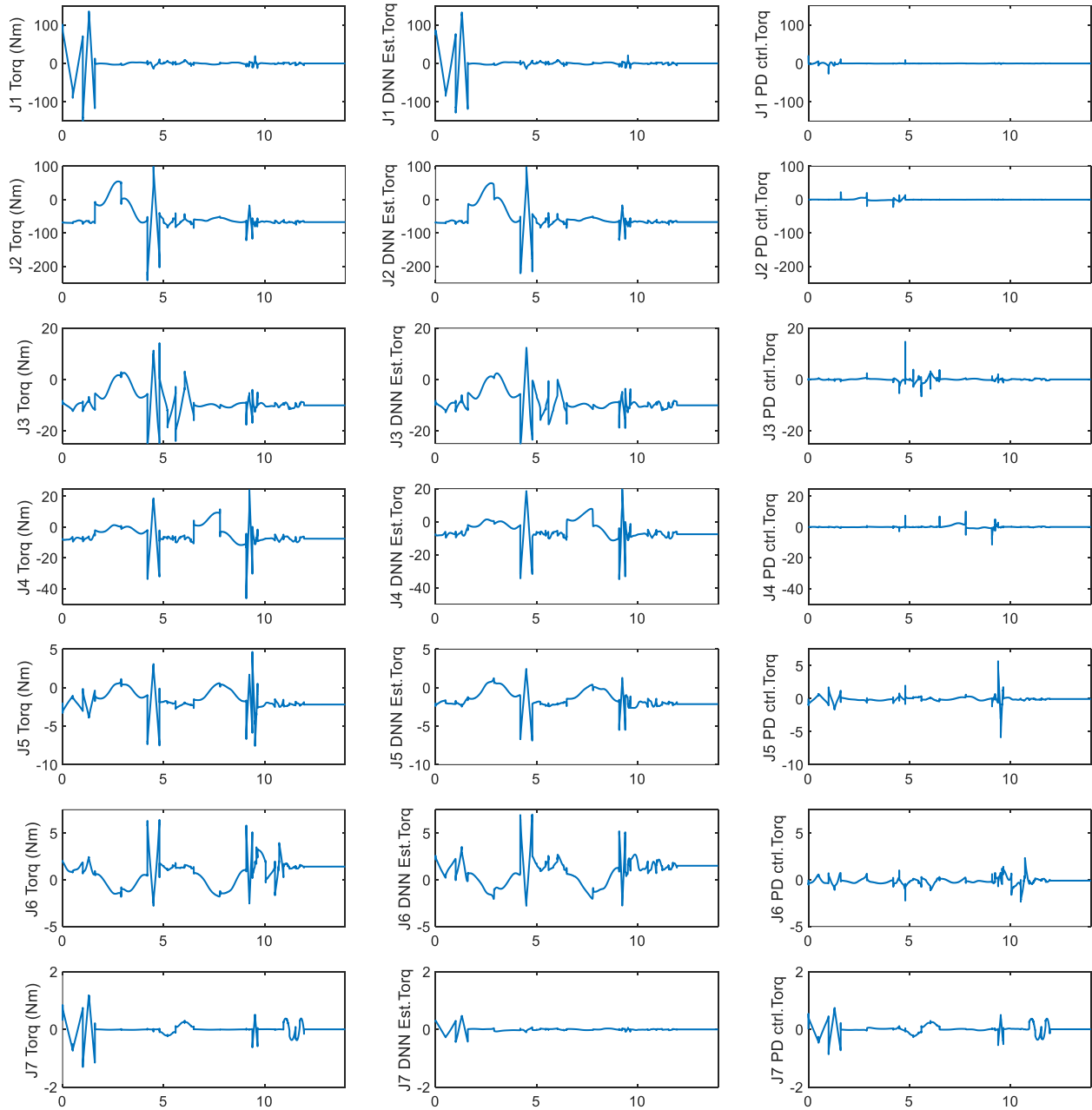


Figure 22 From the left: total Joint torque requirement for sequential joint movements, DNN Predicted torque, PD controller's contribution

Based on the observed results, it can be concluded that the developed deep neural network-based hybrid controller exhibits excellent trajectory tracking performance. The next section will present the robustness of the developed controller to the parameter variations.

## 7. Controller robustness analysis against parameter variations ANOVA

ANOVA, introduced by Ronald Fisher in 1918 [49] is a statistical technique to assess the impact of variations in system parameters on the outputs. User's mass and length were varied and the effects on the trajectory tracking errors were observed to evaluate the robustness of the designed controller.

Statistically,  $P$  value (measures the evidence against the null hypothesis) plays a significant role in assessing the effect of parameter variation on output. Any value of  $P < \textit{significance level}$  (0.005), expresses that at least one observation is affected by the variation of parameter. The one-way ANOVA test is only applicable for normally distributed data, and the sample size needs to be big enough for better performance. Conducted experiment investigate the relation between tracking error and the user's mass or height. Figure 23 and Figure 24 show the tracking error distribution against the change of user's weight and height, it is evident from the figures that all the tracking errors are normally distributed. The  $P$  values of all 7 joints are significantly higher than the significance level (0.005), (Table 4, Table 5) which concludes that the controller's performance is not affected by the variations of weight or height.

The complete form of the variables used in Table 4 and Table 5 are as follows,

*SS* Sum of squares

*df* - Degrees of freedom

*MS* - Mean square

*F* - statistic

*Prob* - p-value

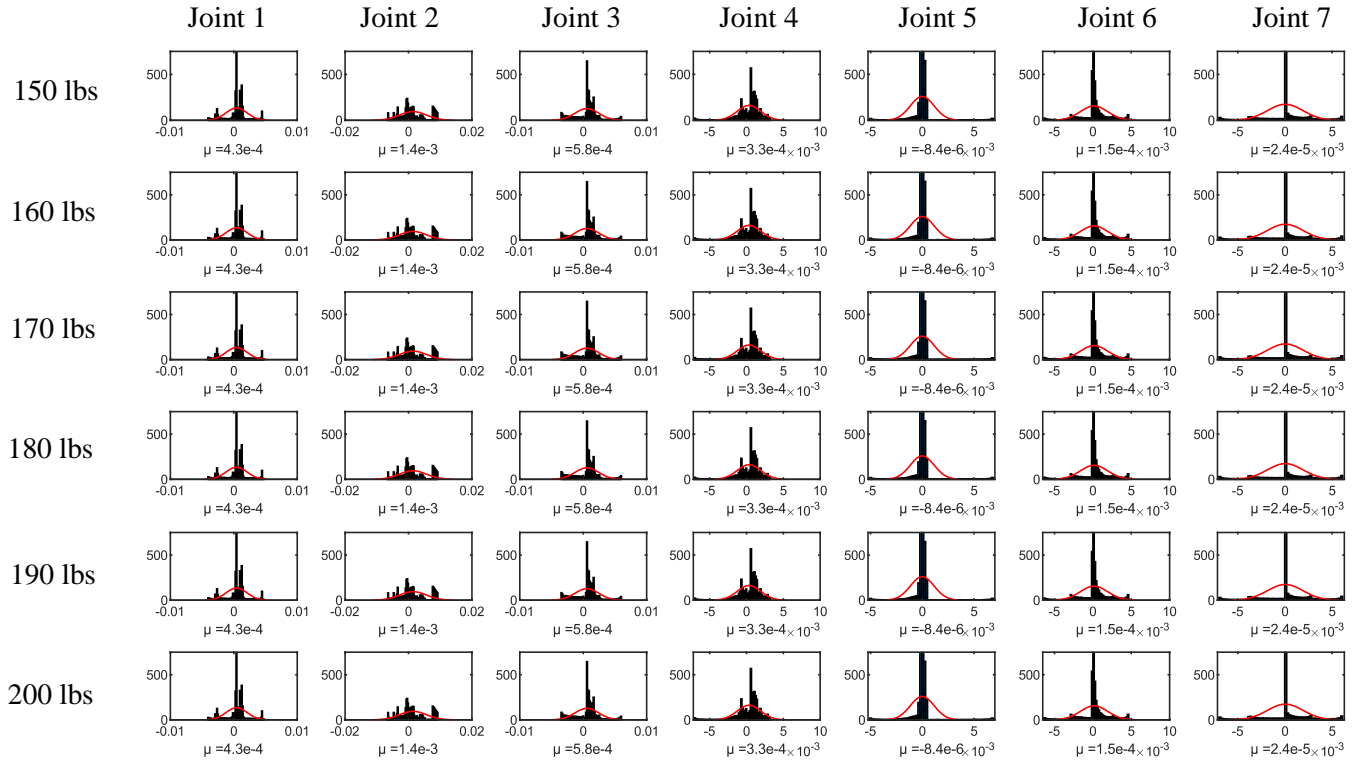
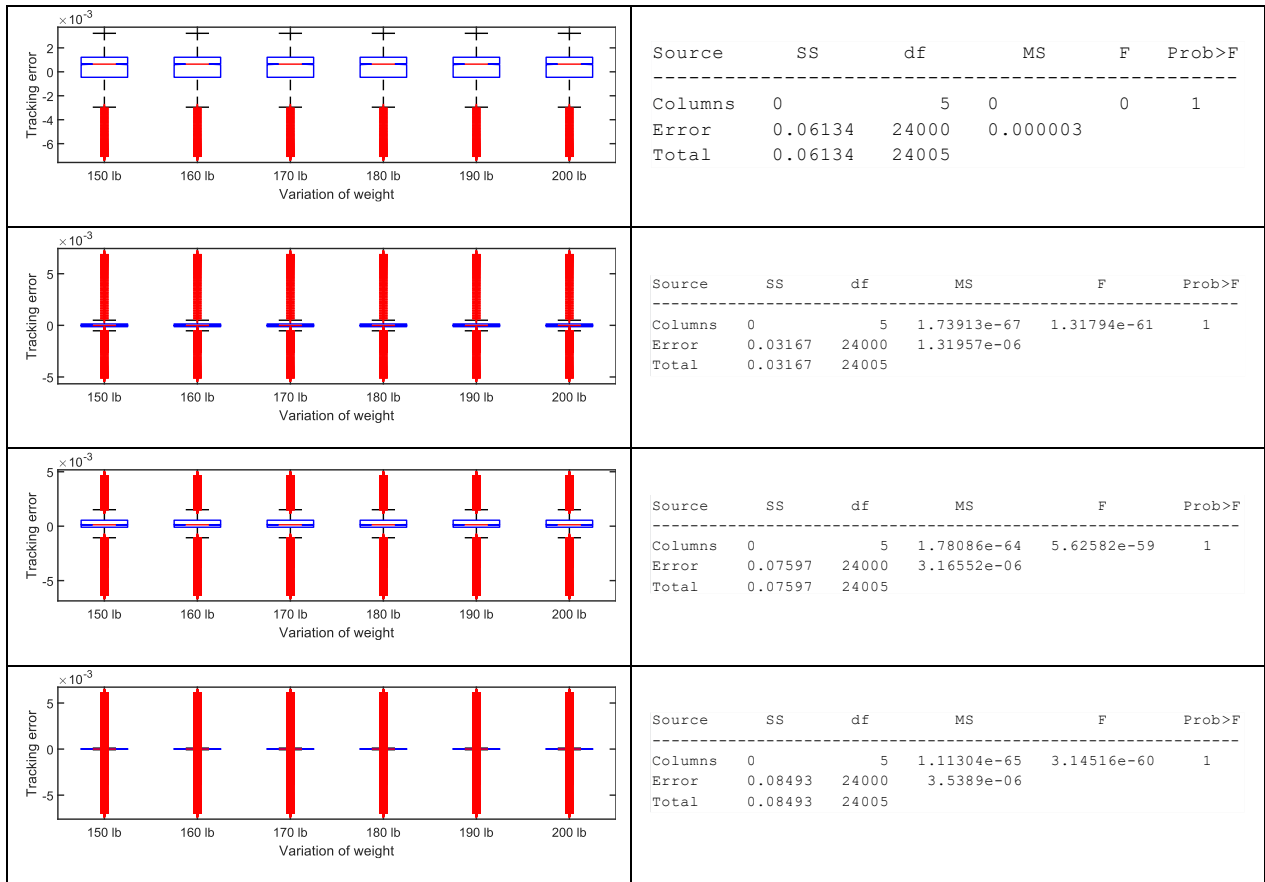


Figure 23 Tracking error distribution concerning weight variation

Table 4 Tracking error variation concerning the user's weight

	<table border="1"> <thead> <tr> <th>Source</th> <th>SS</th> <th>df</th> <th>MS</th> <th>F</th> <th>Prob&gt;F</th> </tr> </thead> <tbody> <tr> <td>Columns</td> <td>0</td> <td>5</td> <td>0</td> <td>0</td> <td>1</td> </tr> <tr> <td>Error</td> <td>0.06521</td> <td>24000</td> <td>0.000003</td> <td></td> <td></td> </tr> <tr> <td>Total</td> <td>0.06521</td> <td>24005</td> <td></td> <td></td> <td></td> </tr> </tbody> </table>	Source	SS	df	MS	F	Prob>F	Columns	0	5	0	0	1	Error	0.06521	24000	0.000003			Total	0.06521	24005			
Source	SS	df	MS	F	Prob>F																				
Columns	0	5	0	0	1																				
Error	0.06521	24000	0.000003																						
Total	0.06521	24005																							
	<table border="1"> <thead> <tr> <th>Source</th> <th>SS</th> <th>df</th> <th>MS</th> <th>F</th> <th>Prob&gt;F</th> </tr> </thead> <tbody> <tr> <td>Columns</td> <td>0</td> <td>5</td> <td>0</td> <td>0</td> <td>1</td> </tr> <tr> <td>Error</td> <td>0.43154</td> <td>24000</td> <td>0.000018</td> <td></td> <td></td> </tr> <tr> <td>Total</td> <td>0.43154</td> <td>24005</td> <td></td> <td></td> <td></td> </tr> </tbody> </table>	Source	SS	df	MS	F	Prob>F	Columns	0	5	0	0	1	Error	0.43154	24000	0.000018			Total	0.43154	24005			
Source	SS	df	MS	F	Prob>F																				
Columns	0	5	0	0	1																				
Error	0.43154	24000	0.000018																						
Total	0.43154	24005																							
	<table border="1"> <thead> <tr> <th>Source</th> <th>SS</th> <th>df</th> <th>MS</th> <th>F</th> <th>Prob&gt;F</th> </tr> </thead> <tbody> <tr> <td>Columns</td> <td>0</td> <td>5</td> <td>0</td> <td>0</td> <td>1</td> </tr> <tr> <td>Error</td> <td>0.08377</td> <td>24000</td> <td>0.000003</td> <td></td> <td></td> </tr> <tr> <td>Total</td> <td>0.08377</td> <td>24005</td> <td></td> <td></td> <td></td> </tr> </tbody> </table>	Source	SS	df	MS	F	Prob>F	Columns	0	5	0	0	1	Error	0.08377	24000	0.000003			Total	0.08377	24005			
Source	SS	df	MS	F	Prob>F																				
Columns	0	5	0	0	1																				
Error	0.08377	24000	0.000003																						
Total	0.08377	24005																							



Variation of tracking errors with subject's height

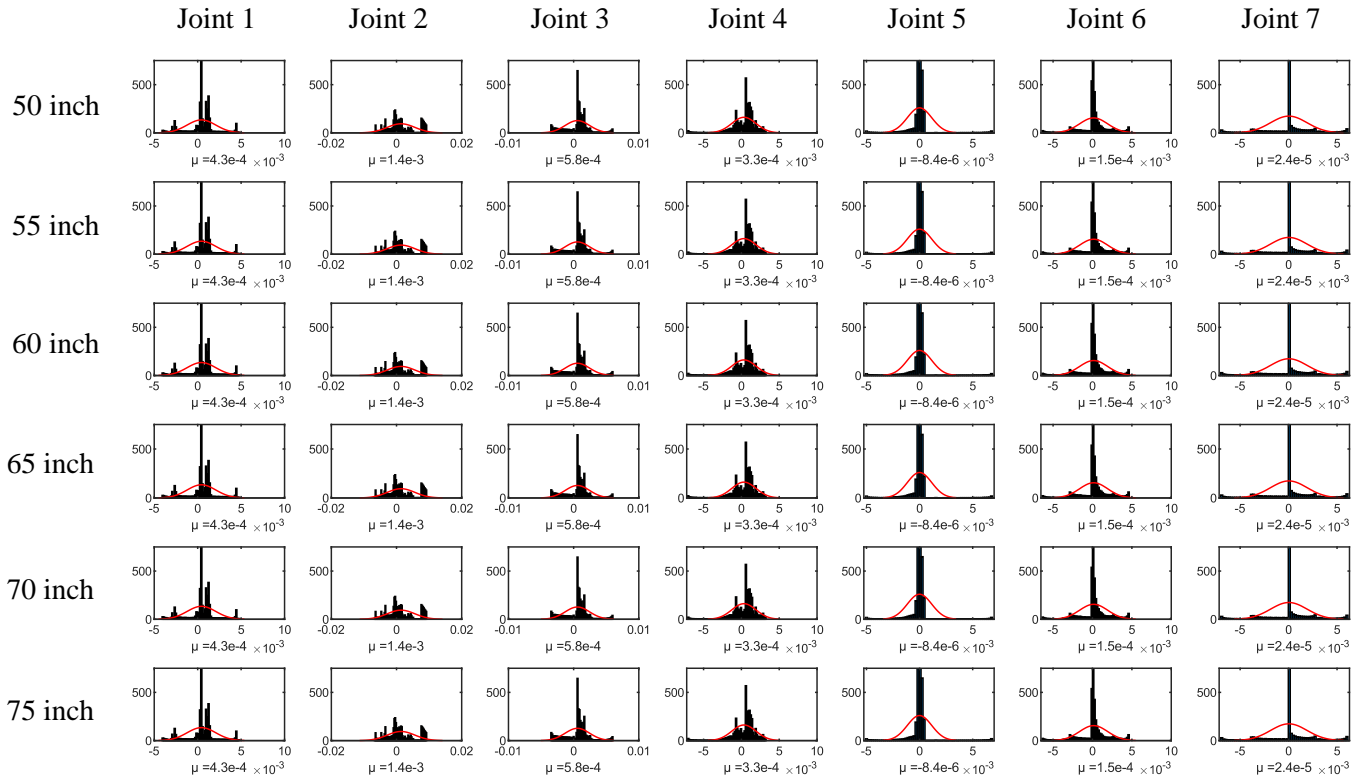
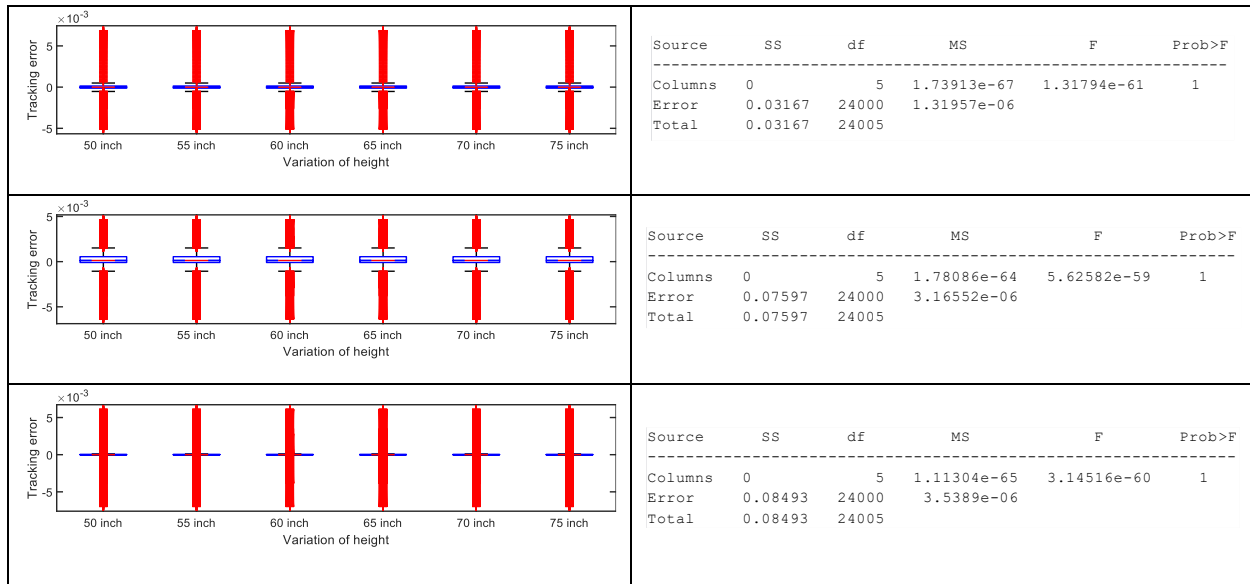


Figure 24 Tracking error distribution concerning the user's height variation

Table 5 Tracking error variation concerning the user's height

<p>Tracking error <math>\times 10^{-3}</math></p> <p>Variation of height</p>	<table border="1"> <thead> <tr> <th>Source</th> <th>SS</th> <th>df</th> <th>MS</th> <th>F</th> <th>Prob&gt;F</th> </tr> </thead> <tbody> <tr> <td>Columns</td> <td>0</td> <td>5</td> <td>0</td> <td>0</td> <td>1</td> </tr> <tr> <td>Error</td> <td>0.06521</td> <td>24000</td> <td>0.000003</td> <td></td> <td></td> </tr> <tr> <td>Total</td> <td>0.06521</td> <td>24005</td> <td></td> <td></td> <td></td> </tr> </tbody> </table>	Source	SS	df	MS	F	Prob>F	Columns	0	5	0	0	1	Error	0.06521	24000	0.000003			Total	0.06521	24005			
Source	SS	df	MS	F	Prob>F																				
Columns	0	5	0	0	1																				
Error	0.06521	24000	0.000003																						
Total	0.06521	24005																							
<p>Tracking error <math>\times 10^{-3}</math></p> <p>Variation of height</p>	<table border="1"> <thead> <tr> <th>Source</th> <th>SS</th> <th>df</th> <th>MS</th> <th>F</th> <th>Prob&gt;F</th> </tr> </thead> <tbody> <tr> <td>Columns</td> <td>0</td> <td>5</td> <td>0</td> <td>0</td> <td>1</td> </tr> <tr> <td>Error</td> <td>0.43154</td> <td>24000</td> <td>0.000018</td> <td></td> <td></td> </tr> <tr> <td>Total</td> <td>0.43154</td> <td>24005</td> <td></td> <td></td> <td></td> </tr> </tbody> </table>	Source	SS	df	MS	F	Prob>F	Columns	0	5	0	0	1	Error	0.43154	24000	0.000018			Total	0.43154	24005			
Source	SS	df	MS	F	Prob>F																				
Columns	0	5	0	0	1																				
Error	0.43154	24000	0.000018																						
Total	0.43154	24005																							
<p>Tracking error <math>\times 10^{-3}</math></p> <p>Variation of height</p>	<table border="1"> <thead> <tr> <th>Source</th> <th>SS</th> <th>df</th> <th>MS</th> <th>F</th> <th>Prob&gt;F</th> </tr> </thead> <tbody> <tr> <td>Columns</td> <td>0</td> <td>5</td> <td>0</td> <td>0</td> <td>1</td> </tr> <tr> <td>Error</td> <td>0.06134</td> <td>24000</td> <td>0.000003</td> <td></td> <td></td> </tr> <tr> <td>Total</td> <td>0.06134</td> <td>24005</td> <td></td> <td></td> <td></td> </tr> </tbody> </table>	Source	SS	df	MS	F	Prob>F	Columns	0	5	0	0	1	Error	0.06134	24000	0.000003			Total	0.06134	24005			
Source	SS	df	MS	F	Prob>F																				
Columns	0	5	0	0	1																				
Error	0.06134	24000	0.000003																						
Total	0.06134	24005																							
<p>Tracking error <math>\times 10^{-3}</math></p> <p>Variation of height</p>	<table border="1"> <thead> <tr> <th>Source</th> <th>SS</th> <th>df</th> <th>MS</th> <th>F</th> <th>Prob&gt;F</th> </tr> </thead> <tbody> <tr> <td>Columns</td> <td>0</td> <td>5</td> <td>0</td> <td>0</td> <td>1</td> </tr> <tr> <td>Error</td> <td>0.06134</td> <td>24000</td> <td>0.000003</td> <td></td> <td></td> </tr> <tr> <td>Total</td> <td>0.06134</td> <td>24005</td> <td></td> <td></td> <td></td> </tr> </tbody> </table>	Source	SS	df	MS	F	Prob>F	Columns	0	5	0	0	1	Error	0.06134	24000	0.000003			Total	0.06134	24005			
Source	SS	df	MS	F	Prob>F																				
Columns	0	5	0	0	1																				
Error	0.06134	24000	0.000003																						
Total	0.06134	24005																							



All the ANOVA results presented on Table 4, Table 5 concludes that the developed controller is highly robust against the system parameter variations.

The next section will present the comparative studies between the developed controller and Sliding mode controller, Computed Torque Controller, Adaptive controller, Linear Quadratic Regulator, and Model Reference Computed Torque Controller.

### 8. Performance comparison of the developed deep neural network based controller with Computed Torque Controller, Model Reference Computed Torque Controller, Sliding Mode Controller, Adaptive controller and Linear Quadratic Regulator

Control systems play a crucial role in robotic systems by providing tracking accuracy and robustness.

This section would provide a comparative study between the developed deep neural network based hybrid controller and some previously developed robot control strategies, namely Computed Torque Controller[8], Model Reference Computed Torque Controller [13], Sliding Mode Controller [14], Adaptive controller [12], Linear Quadratic Regulator [50] while maintaining the same robot dynamics. Our goal is to measure the effectiveness and applicability of the proposed controller.

Figure 25 presents a generalized trajectory tracking performance of the developed Deep neural network based controller, Computed Torque Controller, Model Reference Computed Torque Controller, Sliding Mode Controller, Adaptive controller, Linear Quadratic Regulator. All the controllers provided very high trajectory tracking accuracies, for all cases the trajectory tracking errors were limited to  $1^\circ$ . Due to the presence of a very small amount of trajectory tracking errors, it is difficult to separate the output trajectories from the reference trajectories. The maximum amount of trajectory tracking errors for sequential and simultaneous joint movements using Deep neural network based controller, Computed

Torque Controller, Model Reference Computed Torque Controller, Sliding Mode Controller, Adaptive controller, Linear Quadratic Regulator are shown in Table 6 and Table 7

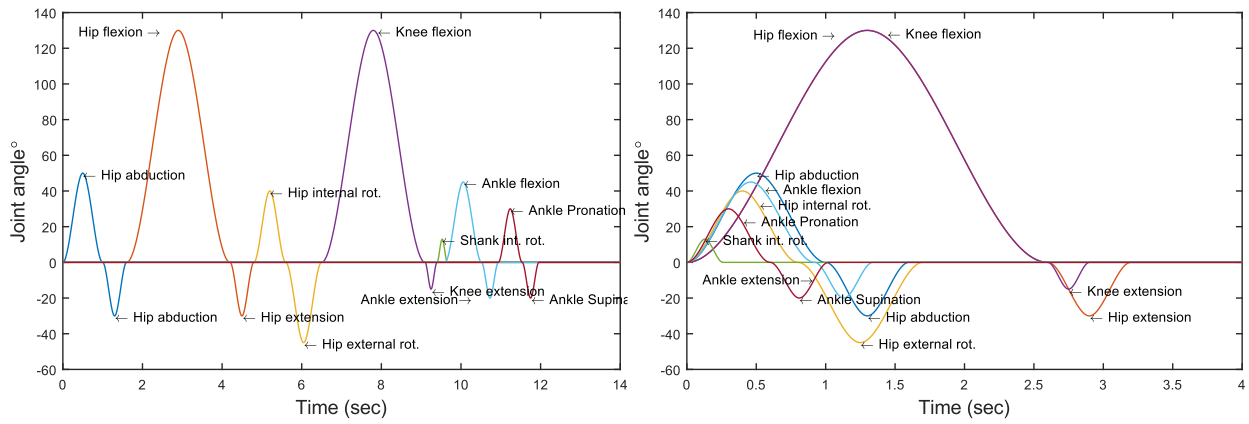


Figure 25 Trajectory tracking performance for the sequential joint movements (left), simultaneous joint movements (right)

Table 6 Maximum values of the trajectory tracking error (Sequential joint movement)

Control technique	Maximum values of the trajectory tracking error (Sequential joint movement)						
	Joint 1	Joint 2	Joint 3	Joint 4	Joint 5	Joint 6	Joint 7
<b>Deep Neural Network based Controller</b>	0.0558°	.01642°	0.0304°	0.1115°	0.0240°	0.0501°	0.0344°
<b>Computed Torque Control (CTC)</b>	0.1175°	0.0909°	0.0991°	0.1637°	0.1694°	0.1441°	0.1590°
<b>Model Reference Computed Torque Controller (MRCTC)</b>	0.1176°	0.0910°	0.0991°	0.1639°	0.1694°	0.1444°	0.1593°
<b>Sliding Mode Controller (SMC)</b>	0.0396°	0.0398°	0.0316°	0.0614°	0.0654°	0.0483°	0.0482°
<b>Adaptive Controller</b>	0.0727°	0.0569°	0.0025°	0.0136°	0.0027°	0.0018°	0.0005°
<b>Linear Quadratic Regulator (LQR)</b>	0.3240°	0.0589°	0.5050°	0.1760°	0.5220°	0.2400°	0.1780°

Table 7 Maximum values of the trajectory tracking error (Simultaneous joint movement)

Control technique	Maximum values of the trajectory tracking error (Simultaneous joint movement)						
	Joint 1	Joint 2	Joint 3	Joint 4	Joint 5	Joint 6	Joint 7
<b>Deep Neural Network based Controller</b>	0.1181°	0.0762°	0.0565°	0.1132°	0.0231°	0.0767°	0.0369°
<b>Computed Torque Control (CTC)</b>	0.1175°	0.0909°	0.1041°	0.1637°	0.1697°	0.1467°	0.1734°
<b>Model Reference Computed Torque Controller (MRCTC)</b>	0.1176°	0.0910°	0.1041°	0.1639°	0.1697°	0.1470°	0.1736°
<b>Sliding Mode Controller (SMC)</b>	0.3966°	0.3988°	0.3165°	0.6142°	0.6545°	0.4838°	0.4842°
<b>Adaptive Controller</b>	0.0378°	0.0762°	0.0365°	0.0208°	0.0726°	0.0022°	0.0010°
<b>Linear Quadratic Regulator (LQR)</b>	0.6450°	0.1060°	0.8000°	0.2800°	0.6180°	0.3010°	0.8640°

All six controllers are based on the same robot dynamics. By comparing the controllers, it has been noticed that all the controller's trajectory tracking accuracy is very high. Developed Deep neural network based controller is highly efficient.

Figure 26 to Figure 31 presents the joint torque requirement for tracking the sequential and simultaneous joint movements. Figure 26 Joint torque requirement for Sequential and Simultaneous Joint Movement using Deep neural network based hybrid controller presents the joint torque requirement for sequential

and simultaneous joint movement using Deep neural network based hybrid controller, Figure 27 shows the joint torque requirement for sequential and simultaneous joint movement using Computed torque controller, Figure 28 depicts the joint torque requirement for sequential and simultaneous joint movement using model reference computed torque controller, Figure 29 presents the joint torque requirement for sequential and simultaneous joint movement using Sliding mode controller, Figure 30 shows the Joint torque requirement for sequential and simultaneous joint movement using Adaptive controller, Figure 31 shows the Joint torque requirement for Sequential and Simultaneous Joint Movement using Linear quadratic regulator. For all the cases the joint peak torques are close and the torque profiles are very similar.

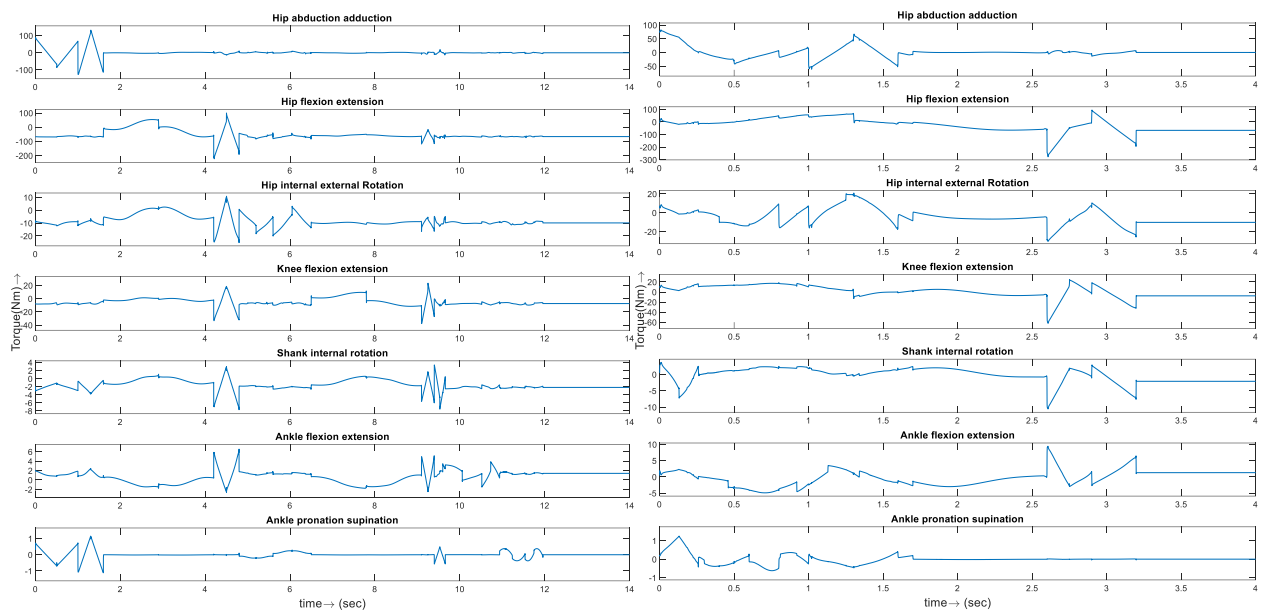


Figure 26 Joint torque requirement for Sequential and Simultaneous Joint Movement using Deep neural network based hybrid controller

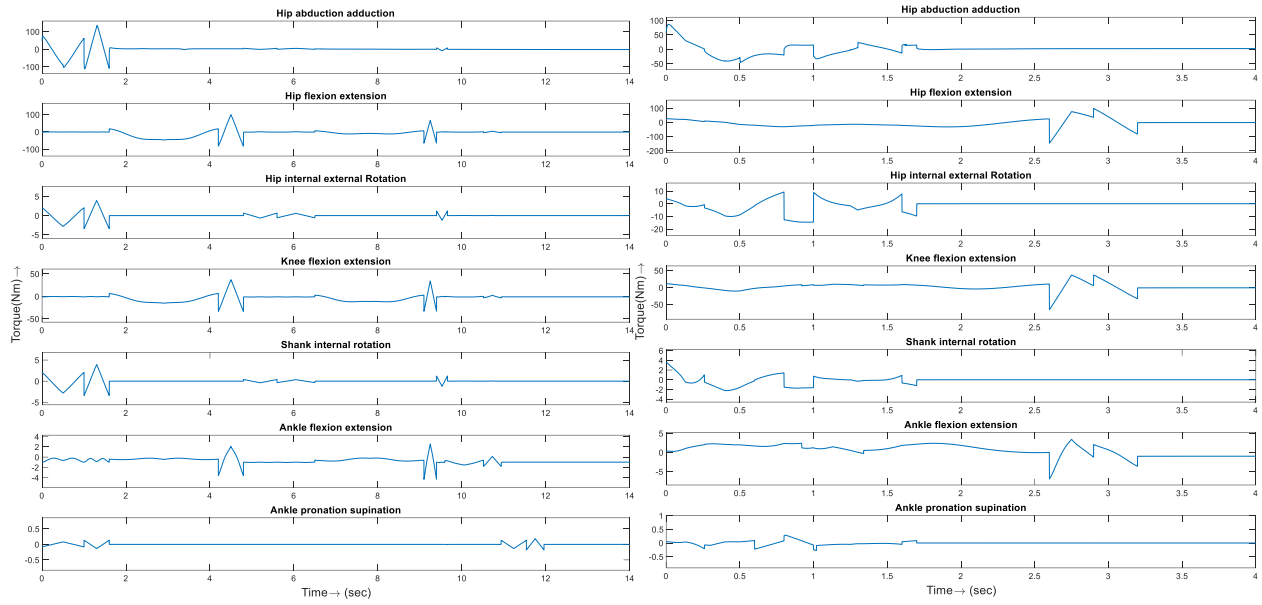


Figure 27 Joint torque requirement for Sequential and Simultaneous Joint Movement using Computed torque controller

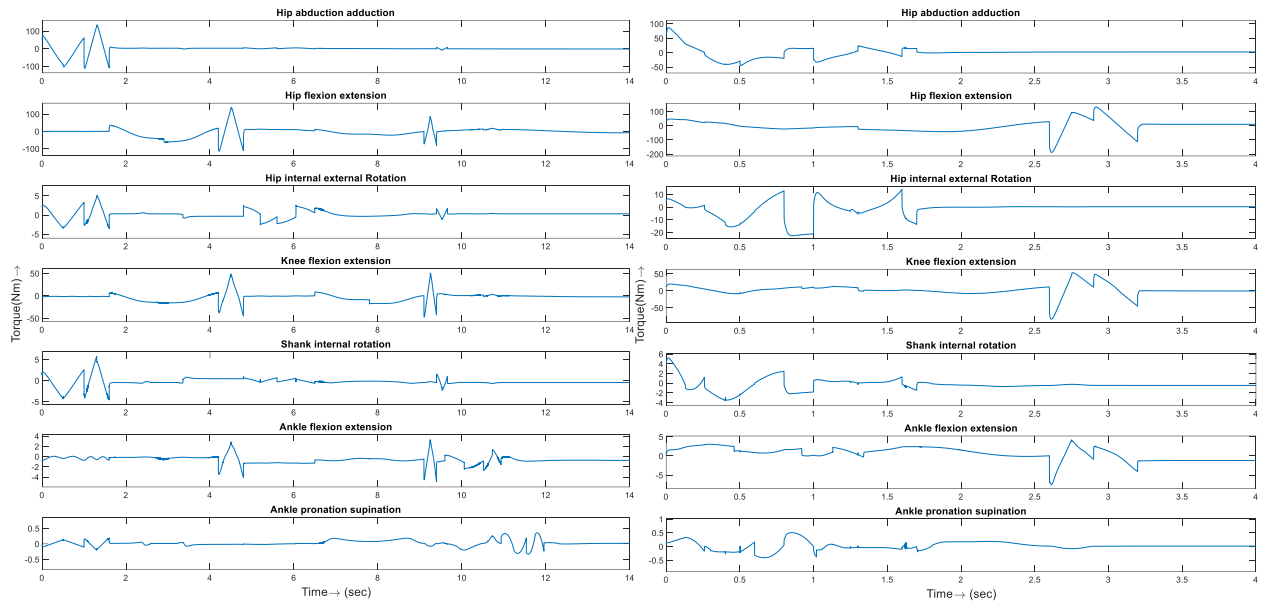


Figure 28 Joint torque requirement for Sequential and Simultaneous Joint Movement using Model reference computed torque controller

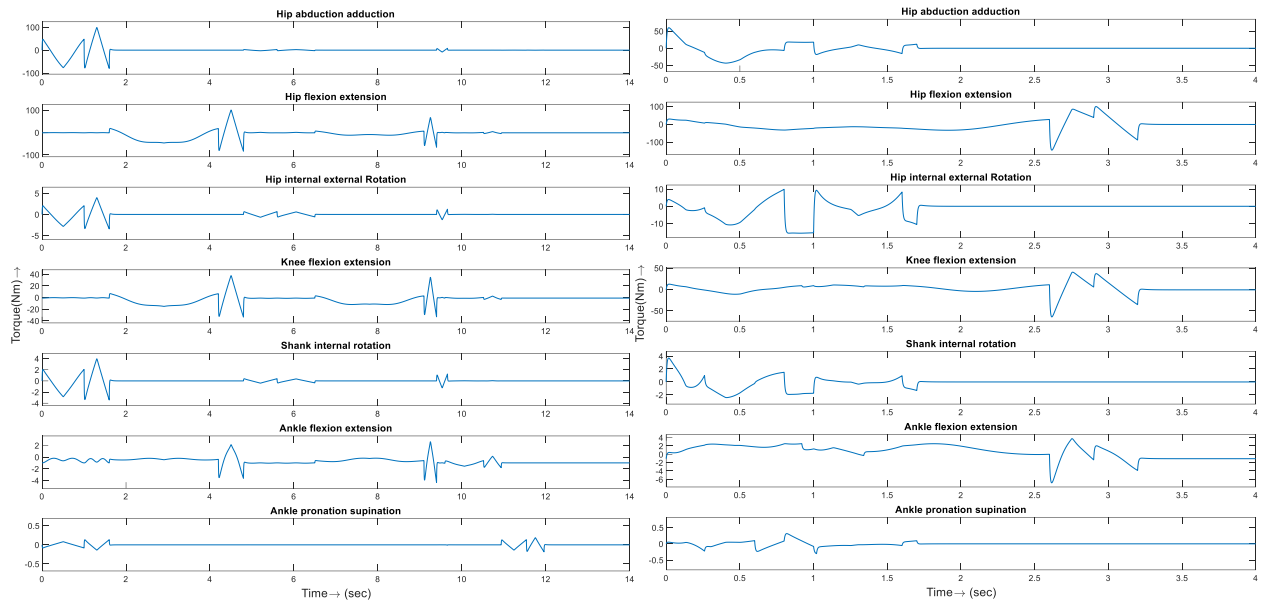


Figure 29 Joint torque requirement for Sequential and Simultaneous Joint Movement using Sliding mode controller

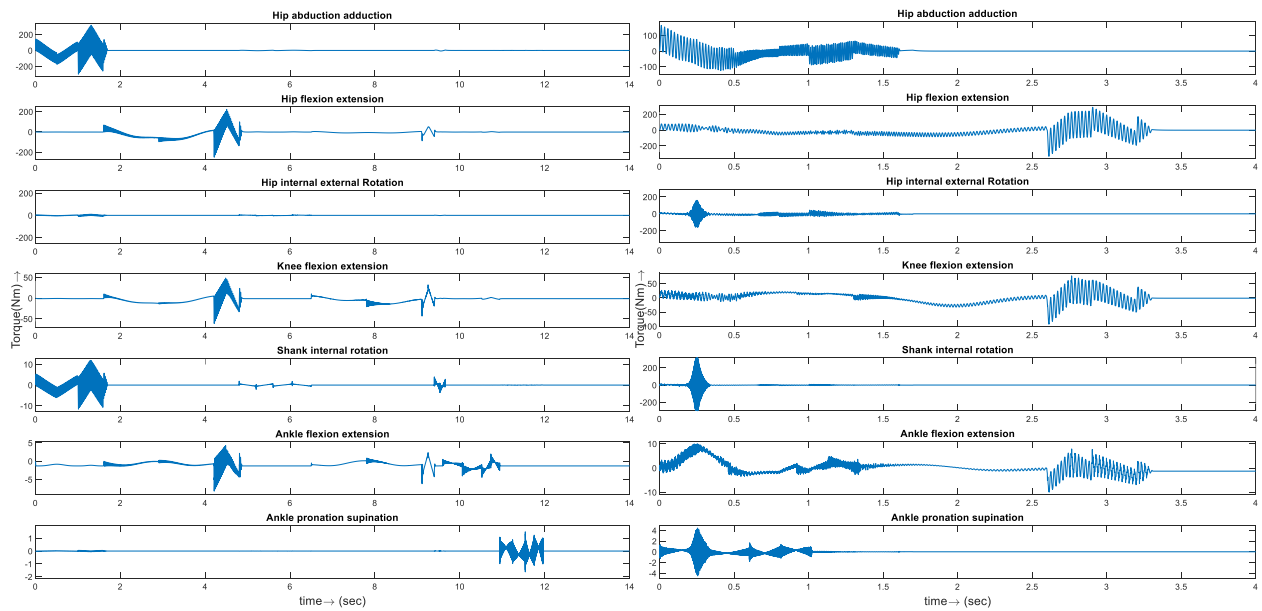


Figure 30 Joint torque requirement for Sequential and Simultaneous Joint Movement using Adaptive controller

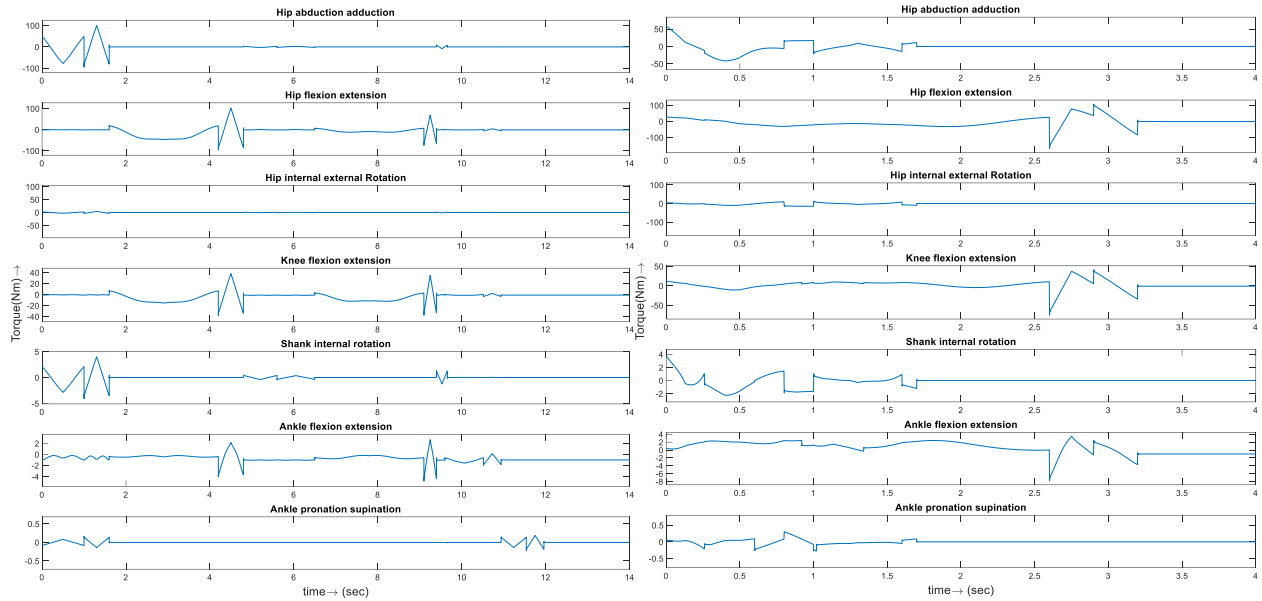


Figure 31 Joint torque requirement for Sequential and Simultaneous Joint Movement using Linear quadratic regulator

Finally, by examining Table 6, Table 7 and Figure 26 to Figure 31 it can be concluded that the developed deep neural network based controller offers very high trajectory tracking accuracy while using torques similar to the conventional controllers.

## 9. Conclusion

Deep neural networks are increasingly being used in the field of dynamic modeling and control. The main reason for the popularity of the deep neural network is that the trained network is computationally light in weight and can model complex dynamic systems accurately. In this article, a human lower extremity exoskeleton robot dynamic model was developed. To control the dynamical model, a computed torque controller was used. The developed dynamical system was simulated for a different combination of trajectories and user weight and height. Reference trajectories, user's weight, height and the exoskeleton robot's joint torques were recorded to train the proposed neural network. A four-layered deep neural network was developed for predicting the robot joint torques based on the reference trajectories, the user's weight, and height. Multiple hidden layers were used to capture the abstract features of the highly nonlinear multiple input output dynamic system. The developed deep neural network-based controller showed very high trajectory tracking accuracy. The stability analysis of the controller is presented. To verify the robustness of the developed controller to parameter variation ANOVA was performed. Finally, the performance of the developed controller was compared with Computed Torque Controller, Model Reference Computed Torque Controller, Sliding Mode Controller, Adaptive controller and Linear Quadratic Regulator while keeping the same robot dynamics.

It is always challenging to develop the perfect model. Besides that for any given dynamic system the model parameter changes over the time. Some adoption mechanism helps to reduce the differences between the dynamic model and the physical system. In the future, a Reinforcement learning method can be added at the top of the developed deep neural network to tune the neural network parameters to improve controller performances.

## Reference

1. Gull, M.A., S. Bai, and T. Bak, A Review on Design of Upper Limb Exoskeletons. *Robotics*, 2020. 9(1): p. 16.
2. Yan, T., et al., Review of assistive strategies in powered lower-limb orthoses and exoskeletons. *Robotics and Autonomous Systems*, 2015. 64: p. 120–136.
3. Rodríguez-Fernández, A., J. Lobo-Prat, and J.M. Font-Llagunes, Systematic review on wearable lower-limb exoskeletons for gait training in neuromuscular impairments. *J Neuroeng Rehabil*, 2021. 18(1): p. 22.
4. Hasan, S. and A. Dhingra, State of the Art Technologies for Exoskeleton Human Lower Extremity Rehabilitation Robots. *Journal of Mechatronics and Robotics*, 2020. 4(1).
5. Siviy, C., et al., Opportunities and challenges in the development of exoskeletons for locomotor assistance. *Nature Biomedical Engineering*, 2023. 7(4): p. 456-472.
6. Zhou, J., S. Yang, and Q. Xue, Lower limb rehabilitation exoskeleton robot: A review. *Advances in Mechanical Engineering*, 2021. 13(4): p. 16878140211011862.
7. Craig, J.J., *Introduction to robotics : mechanics and control*. 2005: Pearson/Prentice Hall, Upper Saddle River, N.J.
8. Hasan, S.K. and A.K. Dhingra, Performance verification of different control schemes in human lower extremity rehabilitation robot. *Results in Control and Optimization*, 2021. 4: p. 100028.
9. Hasan, S.K. and A. Dhingra, Developing a Linear Quadratic Regulator for Human Lower Extremity Exoskeleton Robot. *Journal of Mechatronics and Robotics*, 2022. 6(1).
10. Hasan, S.K. and A.K. Dhingra, Development of a model reference computed torque controller for a human lower extremity exoskeleton robot. *Proceedings of the Institution of Mechanical Engineers, Part I: Journal of Systems and Control Engineering*, 2021. 235(9): p. 1615-1637.
11. Hasan, S.K. and A.K. Dhingra, Development of a sliding mode controller with chattering suppressor for human lower extremity exoskeleton robot. *Results in Control and Optimization*, 2022. 7: p. 100123.
12. Hasan, S.K. and A.K. Dhingra, An adaptive controller for human lower extremity exoskeleton robot. *Microsystem Technologies*, 2021. 27(7): p. 2829-2846.
13. Hasan, S. and A.K. Dhingra, Development of a model reference computed torque controller for a human lower extremity exoskeleton robot. *Proceedings of the Institution of Mechanical Engineers, Part I: Journal of Systems and Control Engineering*, 2021. 235(9): p. 1615-1637.
14. Hasan, S.K. and A.K. Dhingra, 8 Degrees of freedom human lower extremity kinematic and dynamic model development and control for exoskeleton robot based physical therapy. *International Journal of Dynamics and Control*, 2020.

15. Hasan, S.K. and A.K. Dhingra, Biomechanical design and control of an eight DOF human lower extremity rehabilitation exoskeleton robot. *Results in Control and Optimization*, 2022. 7: p. 100107.
16. Goodfellow, I.B.Y.C.A., *Deep learning*. 2016.
17. Dargan, S., et al., A Survey of Deep Learning and Its Applications: A New Paradigm to Machine Learning. *Archives of Computational Methods in Engineering*, 2020. 27(4): p. 1071-1092.
18. Chen, S. and J.T. Wen, Industrial Robot Trajectory Tracking Control Using Multi-Layer Neural Networks Trained by Iterative Learning Control. *Robotics*, 2021. 10(1): p. 50.
19. Zhihong, S. and K. Khorasani, A neural-network-based controller for a single-link flexible manipulator using the inverse dynamics approach. *IEEE Transactions on Industrial Electronics*, 2001. 48(6): p. 1074-1086.
20. Meng, Q., et al., Motion Planning and Adaptive Neural Tracking Control of an Uncertain Two-Link Rigid-Flexible Manipulator With Vibration Amplitude Constraint. *IEEE Transactions on Neural Networks and Learning Systems*, 2021: p. 1-15.
21. Talebi, H.A., K. Khorasani, and R.V. Patel, Neural network based control schemes for flexible-link manipulators: simulations and experiments. *Neural Netw*, 1998. 11(7-8): p. 1357-1377.
22. Yeşildirek, A., M.W. Vandegrift, and F.L. Lewis, A neural network controller for flexible-link robots. *Journal of Intelligent and Robotic Systems*, 1996. 17(4): p. 327-349.
23. Gao, H., et al., Neural Network Control of a Two-Link Flexible Robotic Manipulator Using Assumed Mode Method. *IEEE Transactions on Industrial Informatics*, 2019. 15(2): p. 755-765.
24. Yang, S., et al., An optimal fuzzy-theoretic setting of adaptive robust control design for a lower limb exoskeleton robot system. *Mechanical Systems and Signal Processing*, 2020. 141: p. 106706.
25. Ren, Y., et al., Adaptive Neural-Network Boundary Control for a Flexible Manipulator With Input Constraints and Model Uncertainties. *IEEE Transactions on Cybernetics*, 2021. 51(10): p. 4796-4807.
26. Lin, H., et al., Learning Deep Nets for Gravitational Dynamics With Unknown Disturbance Through Physical Knowledge Distillation: Initial Feasibility Study. *IEEE Robotics and Automation Letters*, 2021. 6(2): p. 2658-2665.
27. Mukhopadhyay, R., et al. Model Learning for Robotic Manipulators using Recurrent Neural Networks. in *TENCON 2019 - 2019 IEEE Region 10 Conference (TENCON)*. 2019.
28. Liu, N., et al., Modeling and Simulation of Robot Inverse Dynamics Using LSTM-Based Deep Learning Algorithm for Smart Cities and Factories. *IEEE Access*, 2019. 7: p. 173989-173998.
29. Liang, B., et al. Robot Arm Dynamics Control Based on Deep Learning and Physical Simulation. in *2018 37th Chinese Control Conference (CCC)*. 2018.

30. Panwar, R. and N. Sukavanam, Trajectory tracking using artificial neural network for stable human-like gait with upper body motion. *Neural Computing and Applications*, 2020. 32(7): p. 2601-2619.
31. Narendra, K.S. and K. Parthasarathy, Identification and control of dynamical systems using neural networks. *IEEE Transactions on Neural Networks*, 1990. 1(1): p. 4-27.
32. Polydoros, A.S., L. Nalpantidis, and V. Krüger. Real-time deep learning of robotic manipulator inverse dynamics. in *2015 IEEE/RSJ International Conference on Intelligent Robots and Systems (IROS)*. 2015.
33. Liu, C., Z. Zhao, and G. Wen, Adaptive neural network control with optimal number of hidden nodes for trajectory tracking of robot manipulators. *Neurocomputing*, 2019. 350: p. 136-145.
34. He, W., Y. Dong, and C. Sun, Adaptive Neural Impedance Control of a Robotic Manipulator With Input Saturation. *IEEE Transactions on Systems, Man, and Cybernetics: Systems*, 2016. 46(3): p. 334-344.
35. Sanner, R.M. and J.J.E. Slotine, Gaussian networks for direct adaptive control. *IEEE Transactions on Neural Networks*, 1992. 3(6): p. 837-863.
36. Wu, Y., et al., Adaptive neural network control of uncertain robotic manipulators with external disturbance and time-varying output constraints. *Neurocomputing*, 2019. 323: p. 108-116.
37. Zhu, Q., Y. Liu, and G. Wen, Adaptive neural network control for time-varying state constrained nonlinear stochastic systems with input saturation. *Information Sciences*, 2020. 527: p. 191-209.
38. Mathworks.com. Friction in contact between rotating bodies. 2020 07/01/2020]; Available from: <https://www.mathworks.com/help/phymod/simscape/ref/rotationalfriction.html>.
39. Mehrer, J., et al., Individual differences among deep neural network models. *Nature Communications*, 2020. 11(1): p. 5725.
40. Marr, B. Deep Learning Vs Neural Networks – What’s The Difference ? ; Available from: <https://bernardmarr.com/deep-learning-vs-neural-networks-whats-the-difference/>.
41. IBM. AI vs. Machine Learning vs. Deep Learning vs. Neural Networks Available from: <https://www.ibm.com/cloud/blog/ai-vs-machine-learning-vs-deep-learning-vs-neural-networks>.
42. Deep Neural Networks. 2023 [cited 2023 06/04/2023]; Available from: [https://www.tutorialspoint.com/python\\_deep\\_learning/python\\_deep\\_learning\\_deep\\_neural\\_networks.htm](https://www.tutorialspoint.com/python_deep_learning/python_deep_learning_deep_neural_networks.htm).
43. Artificial Neural Networks: What they are & why they matter. 06/01/2023 [cited 2023; Available from: [https://www.sas.com/en\\_us/insights/analytics/neural-networks.html](https://www.sas.com/en_us/insights/analytics/neural-networks.html).
44. E, B. and D. B. Performance Analysis and CPU vs GPU Comparison for Deep Learning. in *2018 6th International Conference on Control Engineering & Information Technology (CEIT)*. 2018.
45. Bengio, Y., Learning Deep Architectures for AI. *Found. Trends Mach. Learn.*, 2009. 2(1): p. 1–127.

46. Generate feedforward neural network. [cited 2023 06/01/2023]; Available from: <https://www.mathworks.com/help/deeplearning/ref/feedforwardnet.html>.
47. Gavin, H.P. The Levenberg-Marquardt algorithm for nonlinear least squares curve-fitting problems. 2019.
48. Inc., T.M. Levenberg-Marquardt backpropagation. 2023 [cited 2023 07/06/2023]; Available from: <https://www.mathworks.com/help/deeplearning/ref/trainlm.html>.
49. Fisher, R.A., Statistical Methods for Research Workers, in Breakthroughs in Statistics: Methodology and Distribution, S. Kotz and N.L. Johnson, Editors. 1992, Springer New York: New York, NY. p. 66-70.
50. Hasan, S.K. and A.K. Dhingra, Developing a Linear Quadratic Regulator for Human Lower Extremity Exoskeleton Robot. Journal of Mechatronics and Robotics, 2022.

## List of Figures

Figure 1 Mechatronics architecture of a robot .....	3
Figure 2 Link Frame assignment based on modified D-H parameter .....	7
Figure 3 Internal architecture of the robot model .....	11
Figure 4 Internal architecture of the physical Robot model.....	12
Figure 5 Friction model simulation.....	13
Figure 6 Computed torque control scheme .....	14
Figure 7 Hyperbolic tangent and pure linear activation functions .....	15
Figure 8 Multi-layer Neural network training process.....	17
Figure 9 Architecture of the developed deep neural network .....	18
Figure 10 Developed deep neural network for joint torque estimation.....	19
Figure 11 Hierarchical data generation schematic diagram .....	20
Figure 12 Input and Output data tracing locations in the simulation .....	21
Figure 13 Simultaneous and sequential joint movements (constructed based on the human lower extremity's full ranges of motion [14]) .....	22
Figure 14 Training Neural network .....	23
Figure 15 Control architecture of the Deep neural network-based robot controller .....	23
Figure 16 Control architecture of the hybrid controller .....	24
Figure 17 Trajectory tracking performance (Simultaneous joint movement).....	26
Figure 18 Trajectory tracking Error (Simultaneous joint movement).....	26
Figure 19 From the right: total Joint torque requirement for sequential joint movements, predicted torque, PD controller's contribution .....	27
Figure 20 Trajectory tracking performance (Sequential joint movements) .....	28
Figure 21 Trajectory tracking error (Sequential joint movements).....	29
Figure 22 From the left: total Joint torque requirement for sequential joint movements, DNN Predicted torque, PD controller's contribution .....	30
Figure 23 Tracking error distribution concerning weight variation.....	32
Figure 24 Tracking error distribution concerning the user's height variation .....	34
Figure 25 Trajectory tracking performance for the sequential joint movements (left), simultaneous joint movements (right).....	36
Figure 26 Joint torque requirement for Sequential and Simultaneous Joint Movement using Deep neural network based hybrid controller .....	39
Figure 27 Joint torque requirement for Sequential and Simultaneous Joint Movement using Computed torque controller.....	40

Figure 28 Joint torque requirement for Sequential and Simultaneous Joint Movement using Model reference computed torque controller .....	40
Figure 29 Joint torque requirement for Sequential and Simultaneous Joint Movement using Sliding mode controller .....	41
Figure 30 Joint torque requirement for Sequential and Simultaneous Joint Movement using Adaptive controller .....	41
Figure 31 Joint torque requirement for Sequential and Simultaneous Joint Movement using Linear quadratic regulator .....	42

## List of Tables

Table 1: Human lower extremity DH parameters .....	7
Table 2 Different values of joints velocities, subject's weight and height used for training data generation .....	22
Table 3: Routh Hertz table.....	25
Table 4 Tracking error variation concerning the user's weight.....	32
Table 5 Tracking error variation concerning the user's height.....	34
Table 6 Maximum values of the trajectory tracking error (Sequential joint movement).....	36
Table 7 Maximum values of the trajectory tracking error (Simultaneous joint movement).....	38